國立交通大學

電機學院　電機與控制學程

碩士論文

具有可調變電容補償電流模式遲滯控制技術連續導通模式下的昇壓電源轉換器

Adaptive Capacitor Compensation Control Technique of Hysteretic Current Mode under Continuous Conduction Mode for DC-DC Boost Converters

研究生：楊鴻源

指導教授：陳科宏　博士

中華民國九十八年十二月

具有可調變電容補償電流模式遲滯控制技術連續導通模式下的昇壓電源轉換器

Adaptive Capacitor Compensation Control Technique of Hysteretic Current Mode under Continuous Conduction Mode for DC-DC Boost Converters

研 究 生：楊鴻源　　Student：Hong-Yuan Yang

指導教授：陳科宏　　Advisor：Ke-Horng Chen

國 立 交 通 大 學

電機學院　電機與控制學程

碩 士 論 文

A Thesis

Submitted to Department of Electrical and Computer Engineering

College of Electrical Engineering

National Chiao Tung University

in partial Fulfillment of the Requirements

for the Degree of

Master

in

Electrical and Control Engineering

December 2009

Hsinchu, Taiwan, Republic of China

中華民國九十八年十二月

具有可調變電容補償電流模式遲滯控制技術連續導通模式下的昇壓電源轉換器

研究生：楊鴻源　　指導教授：陳科宏博士

國立交通大學　　電機學院　　電機與控制學程碩士班

摘　要

本論文提出一個以遲滯電流調變控制(modulated hysteretic current control)為基礎的切換式升壓轉換器，它可以改善傳統切換式升壓轉換器受到系統右半平面零點(right-half-plane zero)影響，而無法有快速暫態響應(transient response)的問題。此升壓轉換器本身可以因負載作切換時，自動調整電感電流的充電時間(on-time)，以達到快速移動平均電感電流到期望值進而縮短系統暫態響應時間。除此之外，基於系統存在的右半平面零點的特性，如果適當的動態調整系統補償極點與零點，可以使升壓轉換器在作負載變化時，有極佳的暫態響應，而且回到穩態時，也有足夠的相位邊限，以維持系統的穩定度。經實驗結果顯示，以本論文所提出的架構其設計的升壓轉換器與傳統的遲滯電流控制切換式升壓轉換器比較起來，在負載由輕載轉為重載時，暫態響應時間較傳統方式縮短了 7.2 倍，而在功率消耗方面卻僅僅增加 1%。

關鍵字：遲滯電流調變控制(modulated hysteretic current control)，暫態響應(transient response)，右半平面零點(right-half-plane zero)

Adaptive Capacitor Compensation Control Technique of Hysteresis Current Mode under Continuous Conduction Mode for DC-DC Boost Converters

Student: Hong-Yuan Yang Advisor: Dr. Ke-Horng Chen

Degree Program of Electrical and Computer Engineering
National Chiao-Tung University

Abstract

This paper proposes a modulated hysteretic current control (MHCC) technique to improve transient response of DC-DC boost converters, which suffer from low bandwidth due to the existence of right-half-plane (RHP) zero. The MHCC technique can automatically adjust the on-time value to rapidly increase the inductor current to shorten the transient response time. Besides, based on the characteristic of right-half-plane (RHP) zero, the compensation pole and zero are deliberately adjusted to achieve the system has an ultra-fast transient response in case of load transient condition and an adequate phase margin in steady state. Experimental results show the improvement in transient response is higher than 7.2 times when load current changes from light to heavy or vice versa compared to the conventional boost converter design. The power consumption overhead is merely 1%.

Keywords—modulated hysteretic current control (MHCC), transient response and right-half-plane zero.

誌 謝

首先要感謝我的指導教授 陳科宏博士在這幾年來的細心教導，使得學生在學業與工作領域上都得到相當大的進步，在此對老師獻上最誠摯的感謝。

感謝通泰積體電路公司總經理陳永修先生、林國明副總和同事們的全力支持和鼓勵，使得我在研究所期間，課業及工作得以順利進行。

謝謝我的同事兼同學銘勝的切磋琢磨，讓我在專業上更加精進。

感謝平輝和 Andrea 在 Layout 上的協助以及 802 Lab 學長姐與學弟妹們的幫忙，能夠讓晶片順利下線。

最後要感謝我的父母、岳父母、妹妹雯瑛、月姬，以及親愛的老婆秀玲、慎凌和剛出生的婷聿，你們的支持與讓我能夠安心的完成學業，你們是我最重要的親人。

再一次的謝謝你們 ！

Contents

Figure Captions

Table Captions

Chapter 1
Introduction

The light emission diode (LED) backlight becomes more popular in today's green power mainstream. LED backlight has better colour gamut and consumes less power than cold cathode fluorescent lamp (CCFL) backlight [1] [2]. Besides, the start-up time in LED backlight is smaller than that of CCFL backlight. As a result, today's LCD backlight system gradually uses LED backlight to enhance display quality and power consumption. However, one of serious disadvantages in LED backlight is worse uniformity since LEDs hardly operate at fairly matched light output level due to variations in semiconductor design and technology.

Generally speaking, one of characteristics that may affect image quality is mainly determined by the backlight uniformity. Therefore, the boost converter is widely utilized for LED backlight display systems to step up low input voltage to a high output voltage for driving a number of LEDs in series. The brightness of the LEDs can be easily adjusted by the digital dimming control method to achieve a precise backlighting control. In order to provide a good driving capability for controlling the brightness of LEDs, the boost converter needs to handle large instant load variation in order not to affect the image quality. The design of boost converters depends on the modulation and compensation methods. Owing to low power consumption requirement, the hysteretic current control (HCC) technique is selected as the modulation method for LED backlight [3]. However, the voltage regulation performance of the HCC technique is worse than that of the pulse width modulation (PWM) method [4]. Thus, in the new proposed HCC technique, an error amplifier is utilized to form the voltage loop in order to improve regulation accuracy as illustrated in Fig. 1(a). Besides, a pre-defined current hysteresis window, V_{IW}, can limit the inductor current within it to guarantee a restricted output

voltage ripple as expressed in (1). As a result, the regulation performance and power consumption can be ensured by the new HCC technique.

$$\Delta v_o = \frac{\Delta I_L \cdot L}{2RC_o} + R_{ESR} i_{load} \tag{1}$$

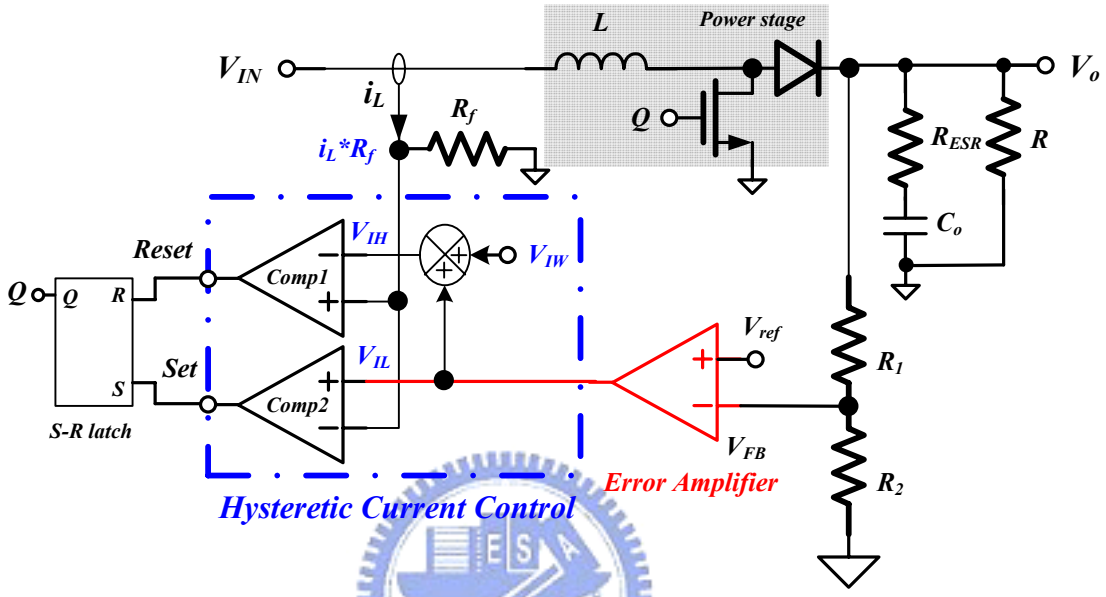

(a)

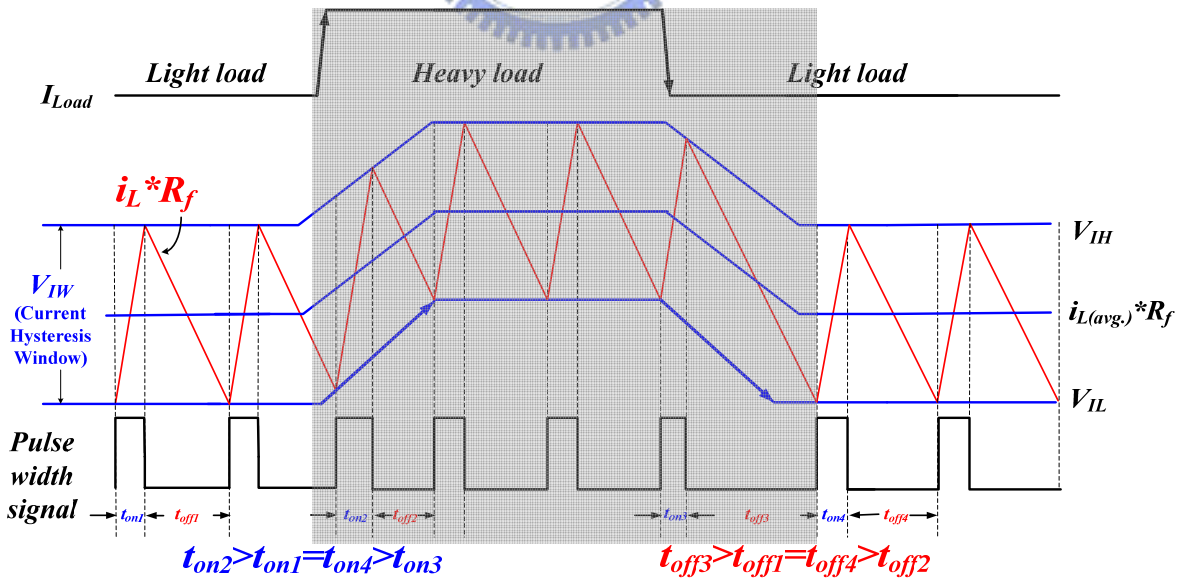

(b)

Fig. 1. (a) The new proposed HCC technique uses an error amplifier to enhance the regulation accuracy. (b) The waveforms of the HCC technique.

Furthermore, the new HCC technique has fast transient response since the trailing and leading edges can rapidly react to the output load variation. As shown in Fig. 1(b), the on time of the pulse width signal adaptively increases or decreases when the load current suddenly increases or decreases, respectively. Similarly, the off time can be modulated to improve the transient response time due to the HCC window controlled by the error amplifier.

Unfortunately, unlike the design of buck converters, the transient response of the boost converter is limited by the existence of a right-half-plane (RHP) zero in the continuous conduction mode (CCM) since the RHP zero remains the same in the design of voltage-mode or current-mode PWM and the HCC technique [5]. In conventional boost converter design, the discontinuous conduction mode (DCM) is widely used in order to get a simple compensation since the RHP zero appears at high frequency in DCM operation. But, the slow response can't meet the requirement of the LED backlight. Thus, the better solution is to speed the transient response without being affected by RHP zero. Hence, the MHCC technique is proposed to improve transient response of DC-DC boost converters in this paper. The MHCC technique can automatically adjust the on-time value to rapidly increase the inductor current to shorten the transient response time. The MHCC technique deliberately adjusts the compensation pole and zero to achieve an ultra-fast transient response in case of load transient condition and an adequate phase margin in steady state.

The organization of this paper is as follows. Chapter 2 shows the small-signal analysis of the HCC technique to propose the compensation method to ensure the system stability. Chapter 3 describes the operation of the proposed MHCC technique. The comparison of transient response is also shown to demonstrate the performance. The deliberated adjustment of pole and zero is shown Chapter 4 to achieve the ultra-fast transient response. Experimental results are shown in Chapter 5 to prove the performance and correctness of the proposed MHCC technique. Finally, a conclusion is made in Chapter 6.

Chapter 2

The Small-Signal Analysis and Compensation in the HCC Technique

In the chapter 2, the topologies and principle of MHCC presented. In section 2.1, the small signal modeling of the HCC technique is introduced including. The closed-loop with the PI compensation is introduced in the section 2.2.

2.1 Small Signal Modeling of the HCC Technique

As depicted in Fig. 2, the HCC technique senses the inductor current and limits it within a hysteresis window, which defines the upper and lower current bands. The inductor current rises to reach the upper band of hysteresis window when the low-side MOSFET turns on during t_{on} period [7]. On the other hand, the inductor current falls to reach the lower band of hysteresis window when the low-side MOSFET turns off during t_{off} period. This HCC technique is simple and has fast dynamic characteristics except for electromagnetic interference (EMI) issue.

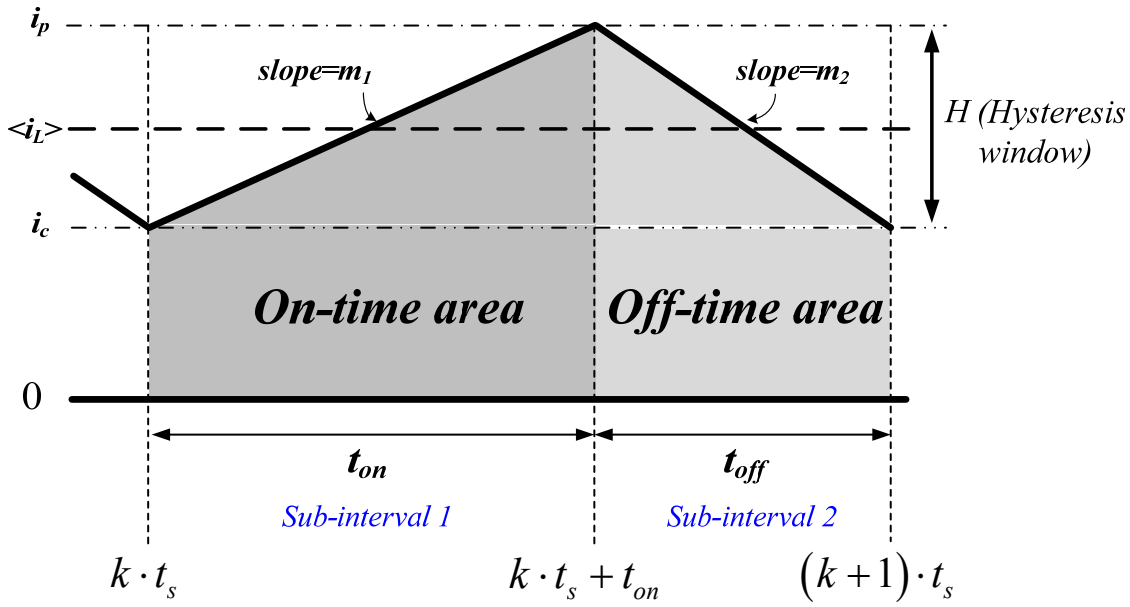

Fig. 2. The inductor current waveform is limited with the hysteresis window defined by the HCC technique.

The switching period t_s as expressed in (2) is equal to the summation of on-time t_{on} and off-time t_{off} in the CCM operation. The value of t_{off} can be written as (3) according to the waveform in the sub-interval 2.

$$t_s = t_{on} + t_{off} \tag{2}$$

$$t_{off} = \frac{LH}{(v_o - v_{in})} \tag{3}$$

The peak inductor current, t_p, can be expressed as (4) by t_{on} and the average inductor current <i_L>.

$$i_p = \langle i_L \rangle + \frac{v_{in}}{2L} t_{on} \tag{4}$$

Considering the small signal analysis, the value of each variable can be written as the summation of the DC term and its perturbation as shown in (5). The duty cycle, d, and its complementary value, d', also are defined in (6)

$$t_s = T_s + \hat{t}_s, \quad t_{on} = T_{on} + \hat{t}_{on}, \text{ and } \quad t_{off} = T_{off} + \hat{t}_{off} = d' t_s \tag{5}$$

$$d = D + \hat{d} \quad \text{and} \quad d' = 1 - d = D' - \hat{d} \tag{6}$$

Hence, (2) and (3) can be re-written as (7) and (8), respectively.

$$\left(T_s+\hat{t}_s\right)=\left(T_{on}+\hat{t}_{on}\right)+\left(T_{off}+\hat{t}_{off}\right) \tag{7}$$

$$T_{off}+\hat{t}_{off}=\frac{LH}{\left(V_o+\hat{v}_o-V_{in}-\hat{v}_{in}\right)} \tag{8}$$

Keeping the first-order ac terms, the small-signal equations can be derived in (9).

$$\hat{t}_s=\hat{t}_{on}+\hat{t}_{off},\ \hat{d}=\frac{\hat{t}_{on}-D\hat{t}_s}{T_s},\text{ and }\ \hat{t}_{off}=-\frac{LH}{\left(V_o-V_{in}\right)^2}\left(\hat{v}_o-\hat{v}_{in}\right) \tag{9}$$

Similarly, $\hat{i}_p$ and $\hat{t}_{on}$ are expressed in (10).

$$\hat{i}_p=\hat{i}_L+\frac{\left(V_{in}\hat{t}_{on}+T_{on}\hat{v}_{in}\right)}{2L}\text{ and }\hat{t}_{on}=\frac{2L}{V_{in}}\left(\hat{i}_p-\hat{i}_L\right)-\frac{T_{on}}{V_{in}}\hat{v}_{in} \tag{10}$$

Therefore, the small-signal duty cycle is derived as (11).

$$\hat{d}=\left(D'\left(\frac{2L}{V_{in}}\left(\hat{i}_p-\hat{i}_L\right)-\frac{T_{on}}{V_{in}}\hat{v}_{in}\right)+\frac{LHD}{\left(V_o-V_{in}\right)^2}\left(\hat{v}_o-\hat{v}_{in}\right)\right)\cdot\left(T_s\right)^{-1} \tag{11}$$

(11) can be simplified as (12) through the use of the DC equivalent equations.

$$\hat{d}=F_m\left(\hat{v}_C-R_f\hat{i}_L\right)+k_f\cdot\hat{v}_{in}+k_r\cdot\hat{v}_o \tag{12}$$

$$F_m=\frac{2DD'}{HR_i},k_f=-\frac{1}{V_o},\text{ and }k_r=\frac{D'}{V_o} \tag{13}$$

As a result, the small-signal model of the boost converter with a hysteretic current mode control is illustrated in Fig. 3 and the control-to-output transfer function is shown in (14). R is the output impedance. R_f is the current sensing gain. R_{ESR} is the equivalent series resistance of output capacitor, C_o.

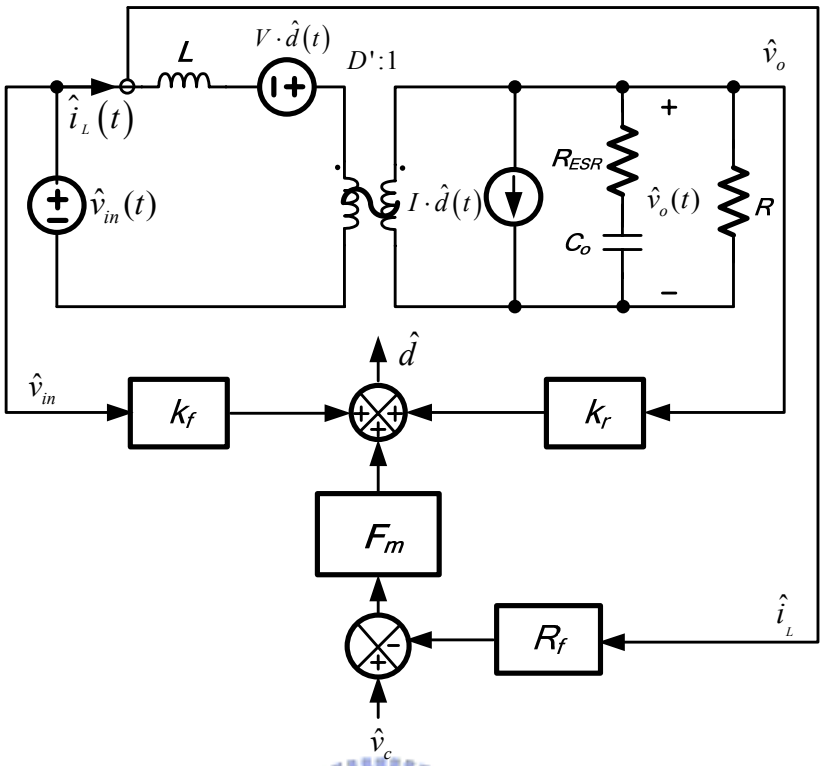

Fig. 3. The small-signal model of the boost converter under the hysteretic current mode control.

$$G_{vc}=\frac{\hat{v}_o}{\hat{v}_c}=\frac{F_m\cdot G_{vd}}{1-k_r\cdot G_{vd}+F_m\cdot G_{id}\cdot R_f} \tag{14}$$

Where $G_{vd}=\left.\frac{\hat{v}_o}{\hat{d}}\right|_{\hat{v}_{in}=0}=\frac{V_o}{D'}\cdot\frac{\left(1-s\frac{L}{D'^2R}\right)\left(1+sR_{ESR}C_o\right)}{1+s\frac{L}{RD'^2}+s^2\frac{LC_o}{D'^2}}$

and $G_{id}=\left.\frac{\hat{i}_L}{\hat{d}}\right|_{\hat{v}_{in}=0}=\frac{2\cdot V_o}{D'^2R}\cdot\frac{\left(1+s\frac{RC_o}{2}\right)}{1+s\frac{L}{RD'^2}+s^2\frac{LC_o}{D'^2}}$ (15)

Furthermore, (14) can be simplified as (16) since $F_m\cdot G_{id}\cdot R_f >> 1-k_r\cdot G_{vd}$

$$G_{vc}=\frac{\hat{v}_o}{\hat{v}_c}=\frac{F_m\cdot G_{vd}}{F_m\cdot G_{id}\cdot R_f}=\frac{1}{R_f}\frac{G_{vd}}{G_{id}}=G_{vc0}\frac{\left(1-\frac{s}{\omega_{z(RHP)}}\right)\left(1+\frac{s}{\omega_{z(ESR)}}\right)}{\left(1+\frac{s}{\omega_{p1}}\right)} \tag{16}$$

$$\text{where } G_{vc0} = \frac{D^{'}R}{2R_f},\ \omega_{p1} = \frac{2}{RC_o}$$
$$\text{and } \omega_{z(RHP)} = \frac{D^{'2}R}{L}, \omega_{z(ESR)} = \frac{1}{R_{ESR}C_o} \tag{17}$$

It is obvious to find that the system contains one dominant pole, ω_{p1}, and two zeros, which include one RHP zero, $\omega_{z(RHP)}$, and one LHP zero, $\omega_{z(ESR)}$. The frequency response of the HCC technique is similar to that of the current-mode PWM technique. In other words, the proportional-integral (PI) compensation is suitable. Basically, the PI compensator has a transfer function as shown in (18). ω_{zc1} is used to cancel the effect of ω_{p1}. ω_{pc1} forms the new dominant pole to determine the system bandwidth. The role of ω_{pc2} is used to decrease the high-frequency gain due to the existence of $\omega_{z(RHP)}$.

$$G_c = G_{c0}\frac{\left(1+\frac{s}{\omega_{zc1}}\right)}{\left(1+\frac{s}{\omega_{pc1}}\right)\left(1+\frac{s}{\omega_{pc2}}\right)} \tag{18}$$

Furthermore, the HCC technique doesn't need slope compensation like that in the current-mode PWM technique. In other words, the compensation in the HCC technique is much simpler than the current-mode PWM technique. However, in both techniques, the existence of the RHP zero seriously affects the system bandwidth.

As illustrated in Fig. 4(a) and (17), the effect of the RHP zero becomes worse at heavy loads. The crossover frequency, ω_c, is generally designed to be smaller than the 10~20% RHP zero, which is the RHP zero at heavy loads, as the illustrated in Fig. 4(b). The output voltage, V_o, has no dip voltage in case of load current variation since the RHP zero is far away from the crossover frequency. That is, the RHP zero has little effect on the dip output voltage. However, the transient response is too slow and thus the output voltage has a large dip voltage due to small bandwidth. On the other hand, an increasing crossover frequency may have a

large dip voltage due to the existence of the RHP zero. However, a large bandwidth can shorten the transient response and get a small undershoot voltage. There exists an optimum ratio between the ω_c and $\omega_{z(RHP)}$ in order to get a smallest dip output voltage, which is labeled as $\Delta V_{o(optimum)}$ at point C. But the phase margin at this optimum dip voltage is not good due to $\omega_{z(ESR)}$ and one high-frequency pole from the compensator. Therefore, the system bandwidth needs to be extended to compensate the dip voltage due to the RHP zero and not be limited by 10~20% RHP zero. The designed value is set at point B, which is about 30% of the RHP zero in this paper for better PM value.

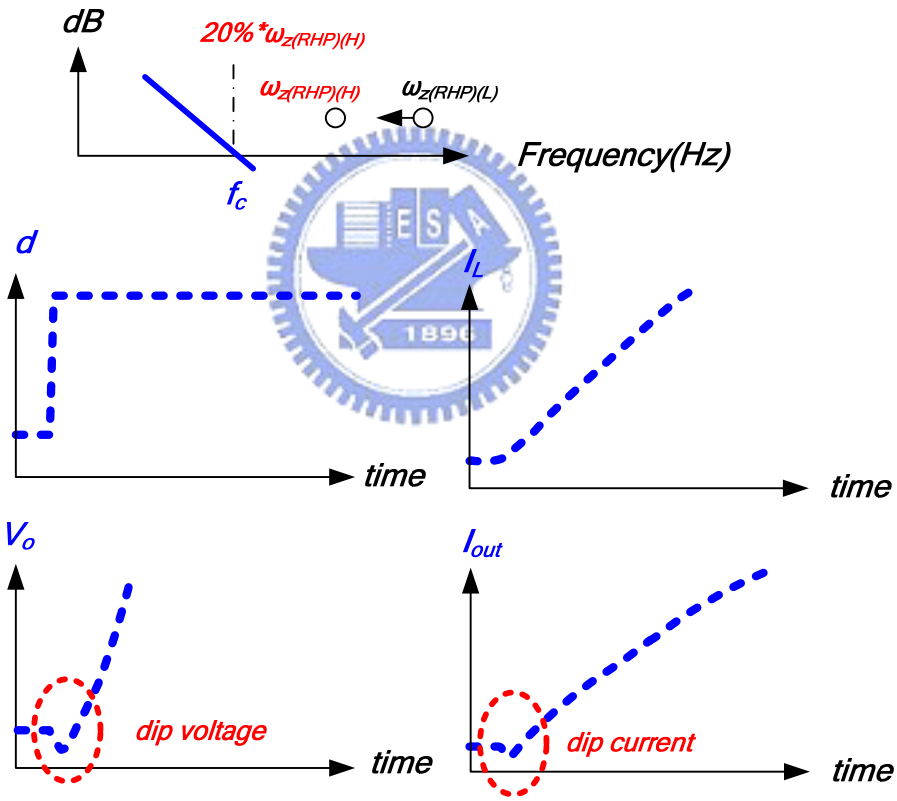

(a)

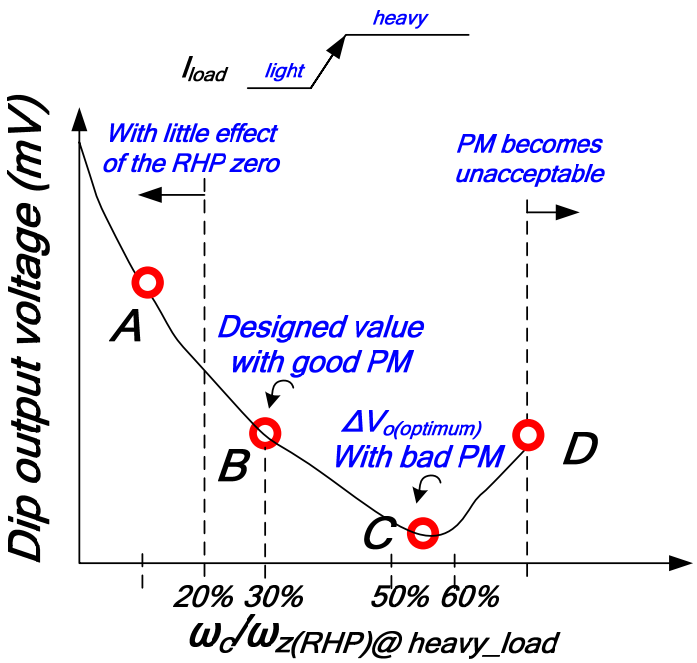

(b)

Fig. 4. The effect of the RHP zero. (a) The step response of the duty may cause a dip output voltage and current due to the existence of the RHP zero. (b) The dip output voltage vs. the ratio of the ω_c and $\omega_{z(RHP)}$.

2.2 The Closed-loop Analysis with the PI Compensation

A closed-loop diagram of the boost converter with the HCC technique is shown in Fig. 5. The loop gain is $T(s)$ as shown in (19). $H(s)$ is the sensor gain, which is equal to $R_2/(R_1+R_2)$. $G_c(s)$ is the compensation transfer function. Generally, $G_c(s)$ is composed of an error amplifier and a PI compensator. The PI compensator contributes one low-frequency pole-zero pair, (ω_{pc1}, ω_{zc1}), and one high-frequency pole, ω_{pc2}.

$$T(s) = G_{vc}(s) \cdot H(s) \cdot G_c(s) \tag{19}$$

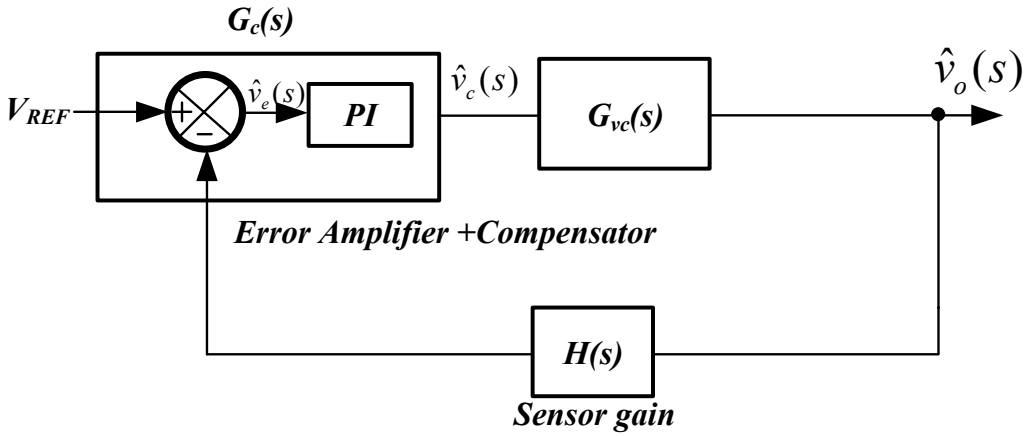

Fig. 5. The simplified feedback system of the HCC regulator.

Therefore, T(s) can be illustrated in Fig. 6 at light and heavy loads. Owing to the decrease of the RHP zero $\omega_{z(RHP)}$ at heavy loads, the compensation zero, f_{zc1}, in the PI compensator is designed to cancel the effect of the system output pole, ω_{p1}, in order to extend the system bandwidth. However, at heavy loads, the crossover frequency is limited by $\omega_{z(RHP)}$, which is represented by a solid dash line in Fig. 6(a). Thus, it is hard to have a good cancellation of the system output pole. According to Fig. 4(b), the ratio of ω_c and $\omega_{z(RHP)}$ has an optimum value when the dip output voltage is the major concern. That is the compensation zero is decided at heavy loads.

On the other hand, the bandwidth becomes worse due to the decrease of ω_{p1} at light loads. As depicted in Fig. 6(b), the compensation zero can be adaptively adjusted within a stable region. The maximum value of ω_{zc1} is determined by the phase margin since there are two poles at low frequencies when the compensation zero is moved toward high frequencies. On the other hand, the minimum value of ω_{zc1} is determined by the minimum value among $\omega_{z(RHP)}$ and ω_{pc2} since the decrease of ω_{zc1} also causes the decrease of ω_{pc2}. As a result, the minimum is no longer decided by $\omega_{z(RHP)}$ since ω_{pc2} is smaller than $\omega_{z(RHP)}$ at light loads. In order to get a better phase margin at light loads, ω_{zc1} needs to be adaptively moved toward the origin at light loads. Consequently**,** an adaptive compensation zero locates high frequencies and low

frequencies at heavy loads and light loads, respectively. However, an adaptive compensation zero can ensure a good phase margin but the transient response is still not improved due to the limitation of low-frequency RHP zero. Thus, the MHCC technique includes an ACC technique to get fast transient response and good phase margin in steady state.

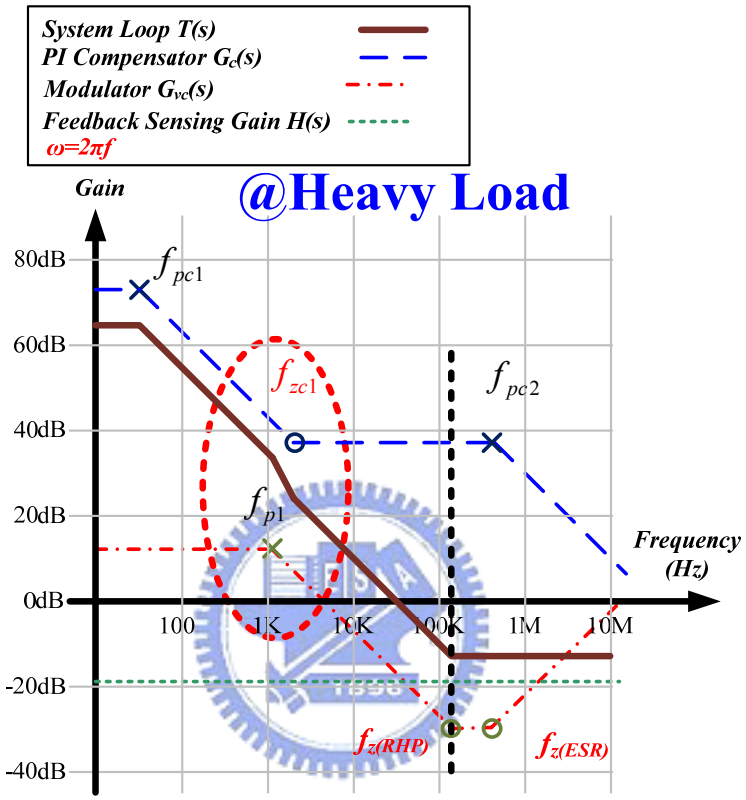

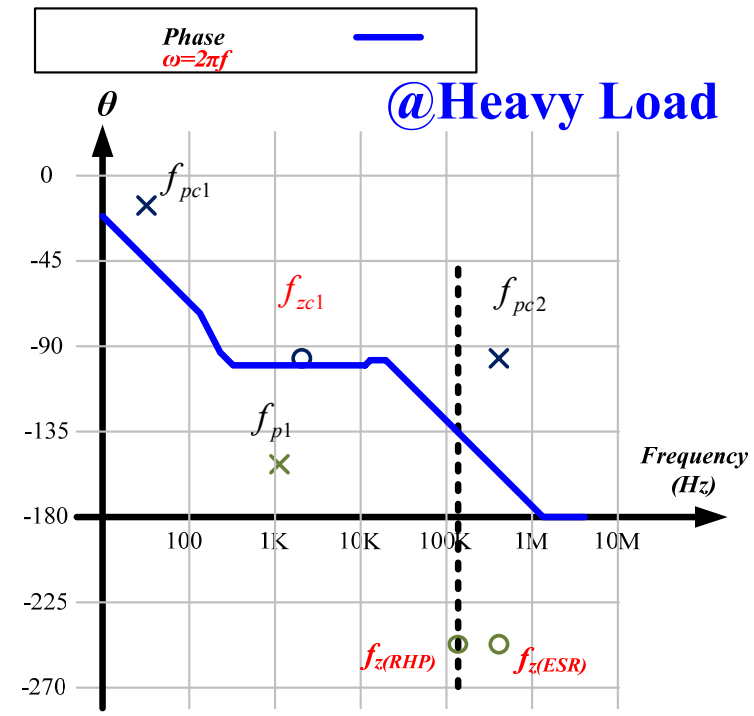
Phase
ω=2πf
@Heavy Load
θ
0
-45
-90
-135
-180
-225
-270
f_{pc1}
f_{zc1}
f_{pc2}
f_{p1}
Frequency
(Hz)
100
1K
10K
100K
1M
10M
$f_{z(RHP)}$
$f_{z(ESR)}$

(a)

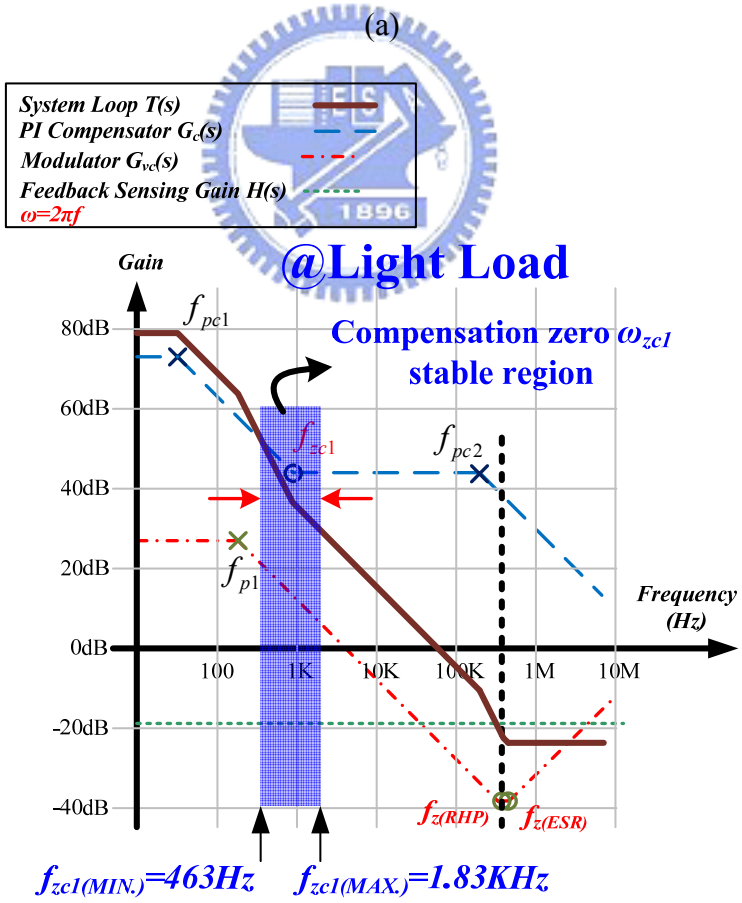
System Loop T(s)
PI Compensator $G_c(s)$
Modulator $G_{vc}(s)$
Feedback Sensing Gain H(s)
ω=2πf
@Light Load
Gain
80dB
60dB
40dB
20dB
0dB
-20dB
-40dB
f_{pc1}
Compensation zero ω_{zc1}
stable region
f_{zc1}
f_{pc2}
f_{p1}
Frequency
(Hz)
100
1K
10K
100K
1M
10M
$f_{z(RHP)}$
$f_{z(ESR)}$
$f_{zc1(MIN.)}$=463Hz
$f_{zc1(MAX.)}$=1.83KHz

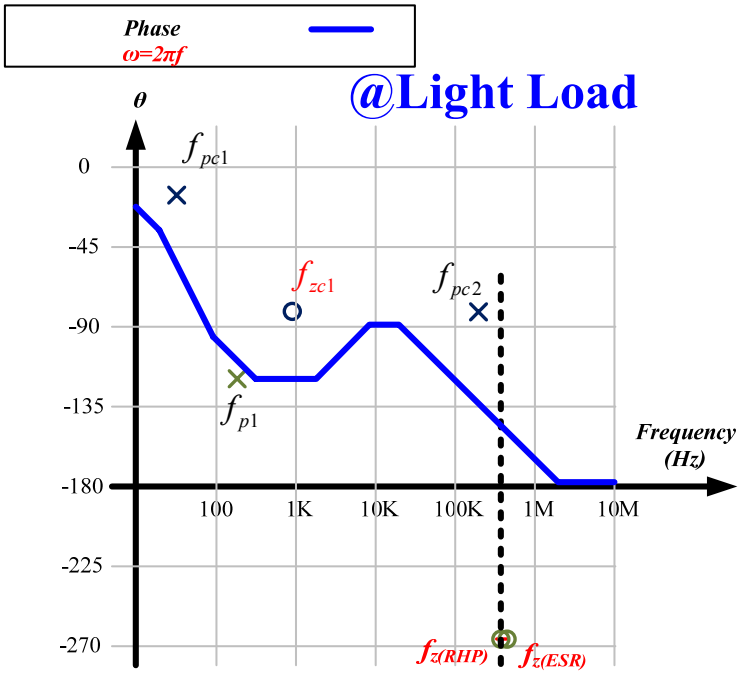

(b)

Fig. 6. The compensated loop gain *T(s)* (a) at light loads and (b) at heavy loads.

Chapter 3

The Proposed MHCC Technique for Fast Transient Response

The proposed MHCC architecture is shown in Fig. 7. It can ensure a limited output ripple and adjust the trailing and leading edges for fast transient response. Besides, the ACC technique can rapidly regulate the output of the error amplifier to speed up the transient response and guarantee a good phase margin in the steady state. The difference voltage between the upper band V_{IH} and the lower band V_{IL} forms the hysteresis current window, which is product of I_{hys} and R_{hys}. V_{IL} is equal to the output voltage V_{eao} of the error amplifier for improving the accuracy of load regulation. The adaptive compensation control technique is composed of the adaptive resistance and capacitance, which are controlled the ACC controller. As a result, the compensation poles and zeros can be adaptively adjusted during load transient and steady state.

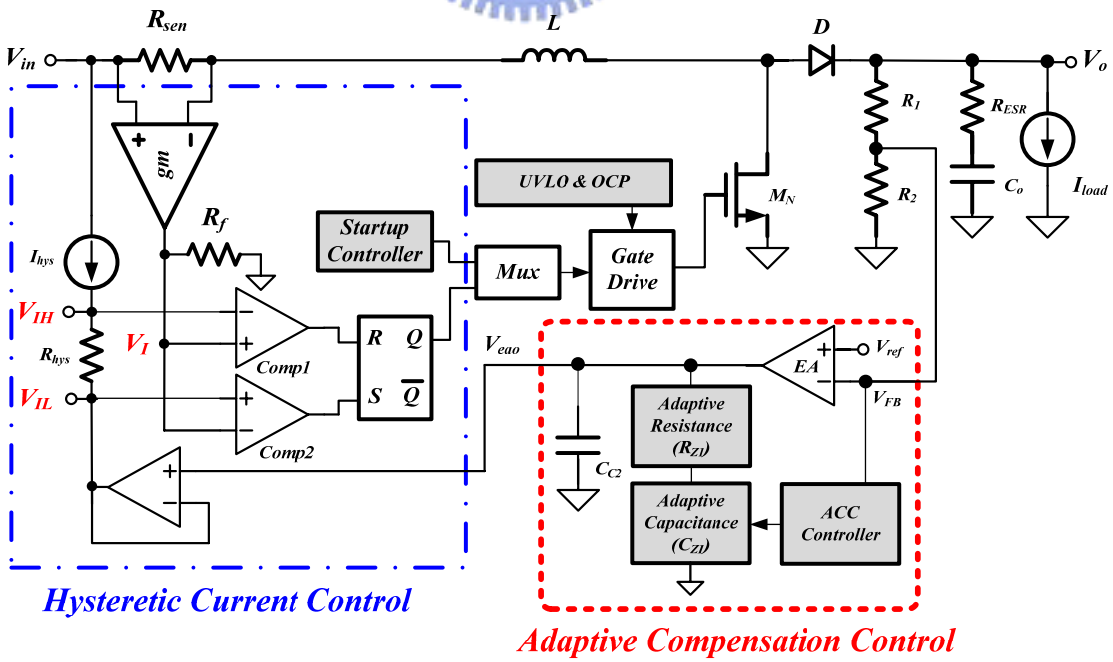

Fig. 7. The system architecture of the proposed boost converter with the proposed MHCC technique.

3.1 The ACC Technique

As depicted in Fig. 8(a), the PI compensator is connected at the output V_{eao} of error amplifier. Since only small on-chip capacitor is allowed in IC fabrication, the small feedback voltage V_{FB} may cause a large voltage variation at V_{eao} since high-frequency compensation zero contributes insufficient phase margin. Therefore, a pseudo large capacitance can be generated through a mirrored ac current, $K*i_c$, connecting to ground as illustrated in Fig. 8(b) [11] [12]. As a result, V_{eao} can have a stable settling behavior since a large transient current can be re-directed to ground. Similar to the off-chip compensation zero, a pseudo low-frequency compensation zero is used to cancel the effect of the output system pole. As mentioned above, the bandwidth is small due to the RHP zero.

In Fig. 8(c), the ACC technique modifies the pseudo compensation poles and zeros to get a small dip output voltage and fast transient response time. According to Fig. 4(b), the ratio of ω_c to $\omega_{z(RHP)}$ can be increased for a short period to get a higher bandwidth and the dip output voltage will not be increased too much when the operation point from B toward higher ratio of ω_c to $\omega_{z(RHP)}$. That is the fast transient period will push the operation point from point B to C, and to D. After the fast transient period, it is pushed back to point B, again, to ensure better PM value. The fast transient period only occupies one fraction of the transient period. The dip output voltage can be smaller than that without the ACC technique. Therefore, the value of V_{eao} can be rapidly settled to its stable level and thus the MHCC technique can achieve a fast transient response and small dip output voltage without being limited by the RHP zero.

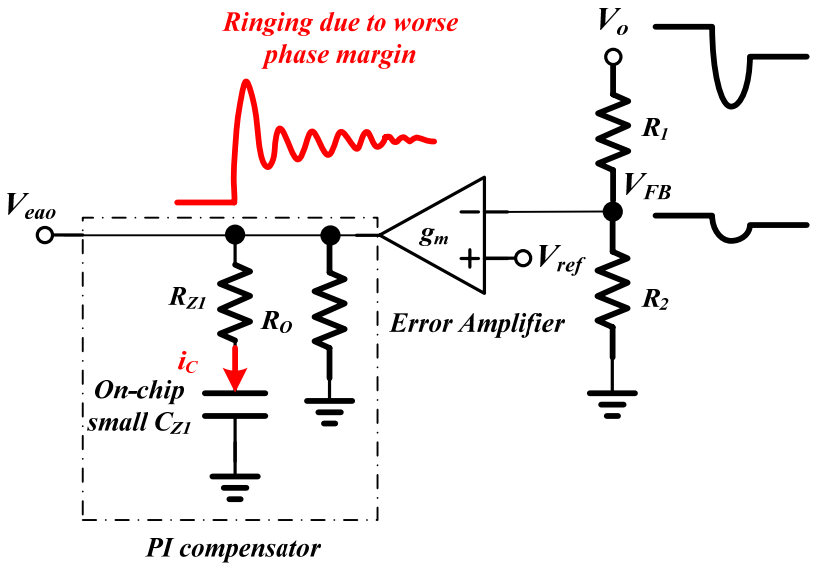
Ringing due to worse
phase margin
V_o
R_1
V_{FB}
V_{eao}
g_m
V_{ref}
R_2
R_{Z1}
R_O
Error Amplifier
i_C
On-chip
small C_{Z1}
PI compensator

(a)

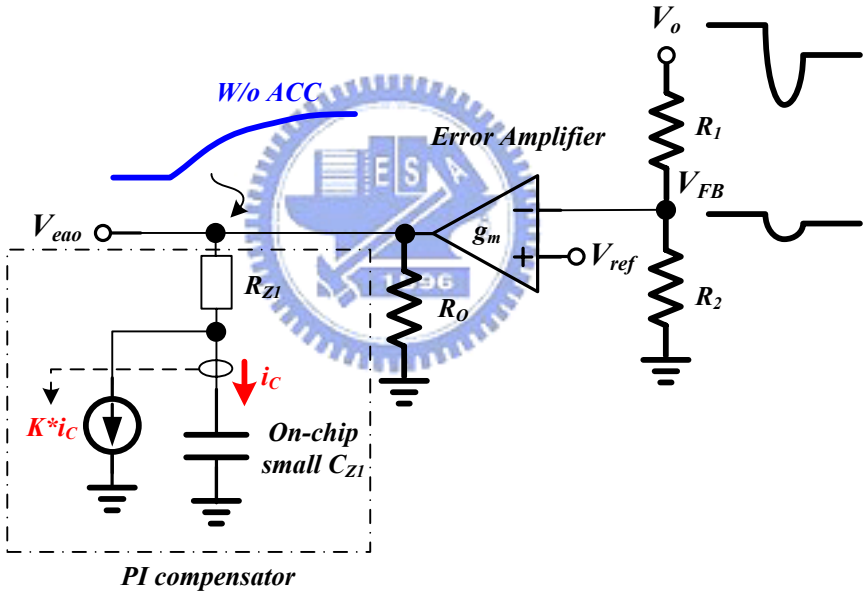
V_o
W/o ACC
Error Amplifier
R_1
V_{FB}
V_{eao}
g_m
V_{ref}
R_{Z1}
R_O
R_2
i_C
$K*i_C$
On-chip
small C_{Z1}
PI compensator

(b)

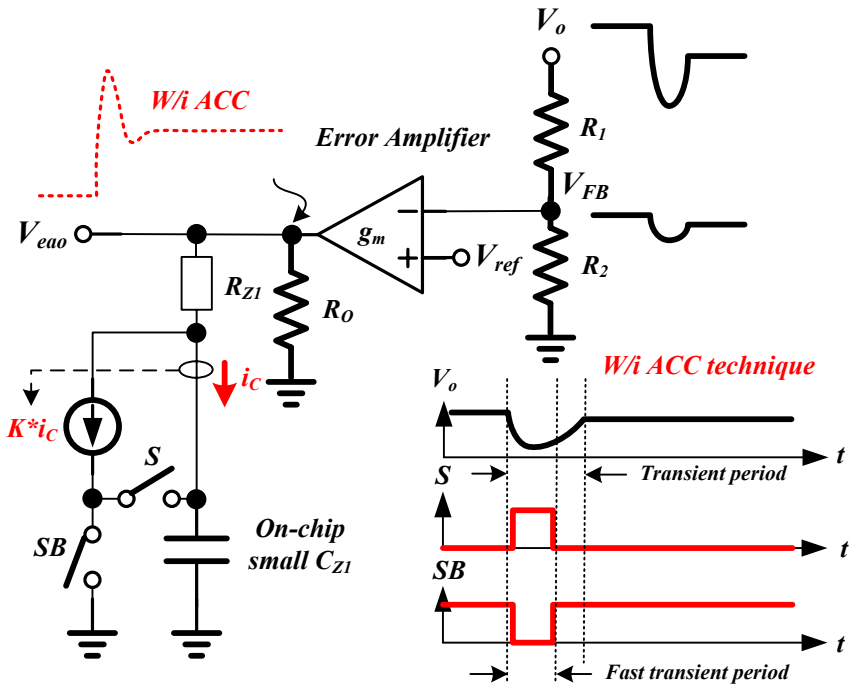

(c)

Fig. 8. The PI compensator (a) with a small on-chip capacitor, (b) with the pseudo capacitance, and (c) with the ACC technique.

The operation of the ACC technique needs to carefully control compensation poles and zeros during the fast transient period. Basically, the fast transient period contains two stages, which are the transient 1 and the transient 2 stages. At the transient 1 stage, the mirrored ac current is fully re-directed to the small on-chip capacitor to rapidly recovery the voltage level of V_{eao}. After the transient 1 stage, the transient 2 stage needs to detect the valley point of the dip output voltage in order to pull back the compensation poles and zeros to the position that ensures the system has a better PM value. The compensation poles and zeros controlled by the ACC technique are shown in Fig. 9 (a) and (b) when load current changes from light to heavy and vice versa.

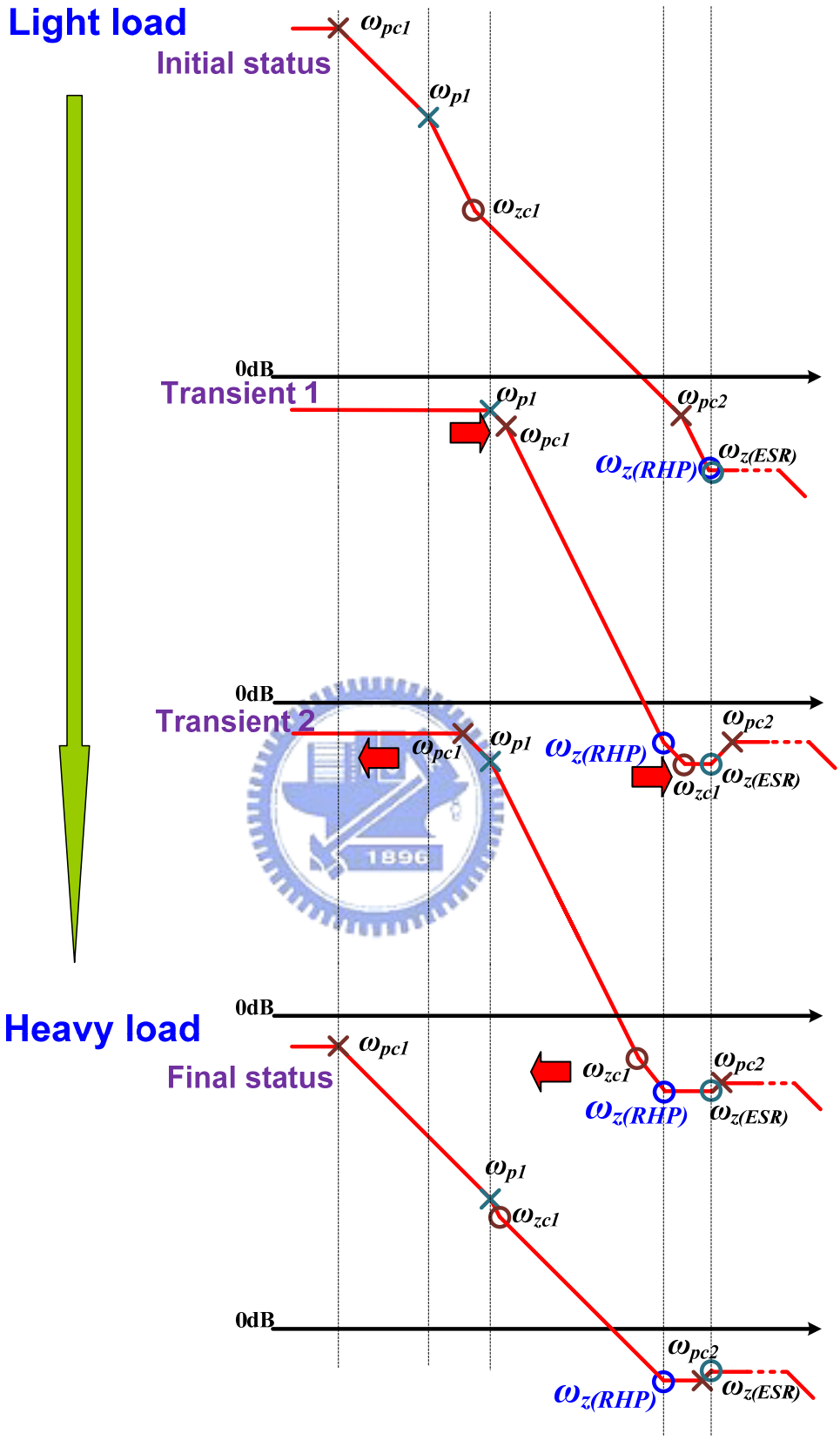
Light load
Initial status
ω_{pc1}
ω_{p1}
ω_{zc1}
0dB
Transient 1
ω_{p1}
ω_{pc1}
ω_{pc2}
$\omega_{z(ESR)}$
$\omega_{z(RHP)}$
0dB
Transient 2
ω_{pc1}
ω_{p1}
$\omega_{z(RHP)}$
ω_{pc2}
ω_{zc1}
$\omega_{z(ESR)}$
0dB
Heavy load
Final status
ω_{pc1}
ω_{zc1}
ω_{pc2}
$\omega_{z(RHP)}$
$\omega_{z(ESR)}$
ω_{p1}
ω_{zc1}
0dB
ω_{pc2}
$\omega_{z(RHP)}$
$\omega_{z(ESR)}$

(a)

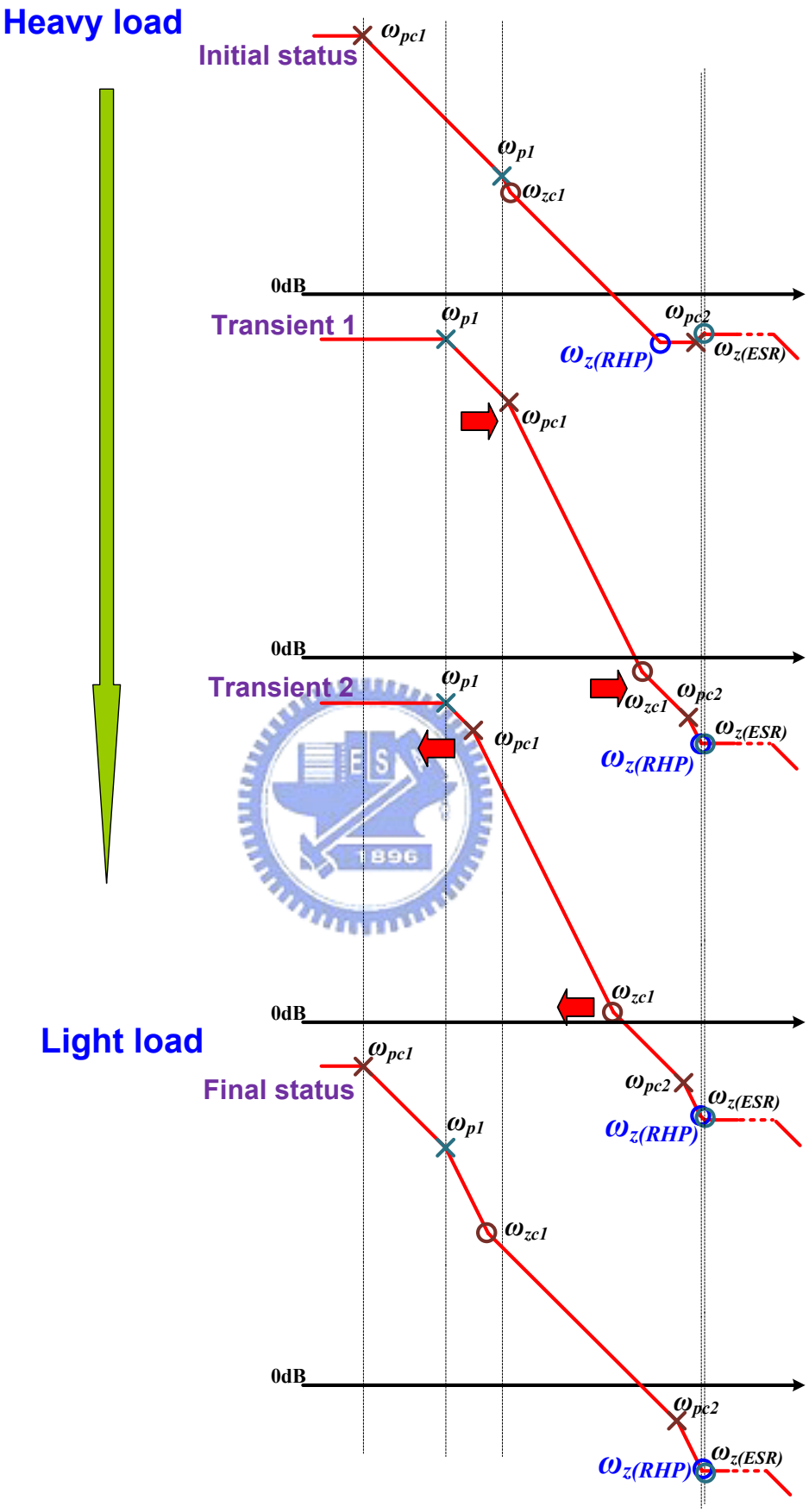
Heavy load
Initial status
ω_{pc1}
ω_{p1}
ω_{zc1}
0dB
Transient 1
ω_{p1}
ω_{pc2}
$\omega_{z(RHP)}$
$\omega_{z(ESR)}$
ω_{pc1}
0dB
Transient 2
ω_{p1}
ω_{zc1}
ω_{pc2}
ω_{pc1}
$\omega_{z(ESR)}$
$\omega_{z(RHP)}$
ω_{zc1}
0dB
Light load
Final status
ω_{pc1}
ω_{pc2}
$\omega_{z(ESR)}$
$\omega_{z(RHP)}$
ω_{p1}
ω_{zc1}
0dB
ω_{pc2}
$\omega_{z(ESR)}$
$\omega_{z(RHP)}$

(b)

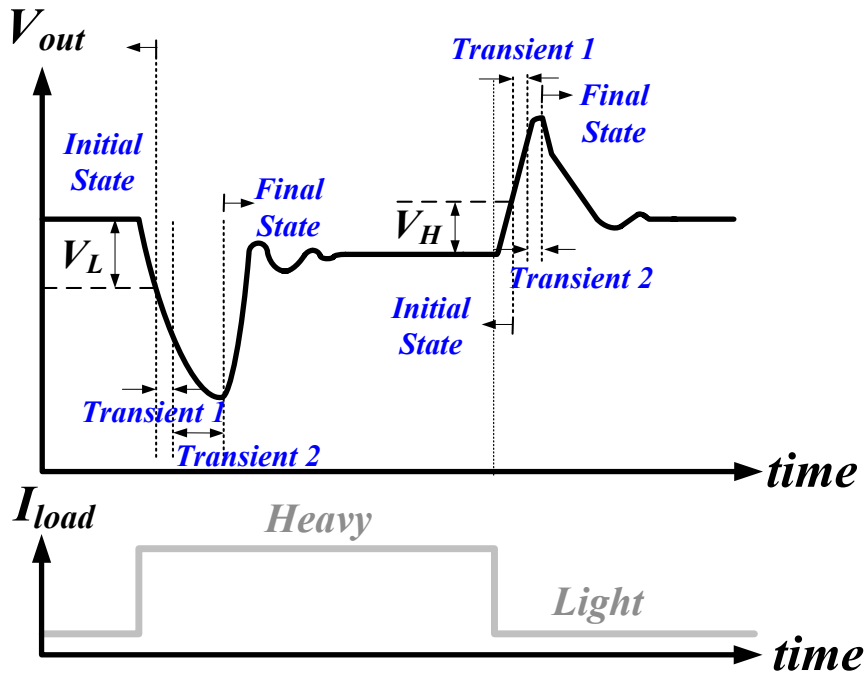

(c)

Fig. 9. (a) The compensation poles and zeros controlled by the ACC technique when load current changes from light to heavy. (b) The compensation poles and zeros controlled by the ACC technique when load current changes from heavy to light. (c) The load transient waveforms controlled by the MHCC technique.

3.2 The Compensation of the Modulation Techniques

The switching frequency of PWM mode is fixed and the switch has to turn on and off every switching cycle. The recovery time takes a longer time as shown in Fig. 10(a) when the output current changes from light to heavy. On the other hand, the inductor current in the HCC technique is controlled within two boundaries i_c, which is determined by the error amplifier, and i_c +ΔI as depicted in Fig. 10(b). ΔI is the current hysteresis window. The recovery time can be shortened since the on-time value will not be limited by the maximum on-time value in the PWM control technique. The switching period can be extended and thus the inductor current can be rapidly increased to the regulated level. The current of i_{l_sub1} gets more time to reach the boundary i_c +ΔI. The system frequency of the boost converter becomes slow when load current changes from light to heavy. This is the reason why the

recovery time of the HCC technique is faster than that of the current-mode PWM technique.

The fast recovery of i_c can speed up the transient response time. Therefore, the proposed MHCC technique rapidly regulates the output of the error amplifier in order to shorten the transient response time. However, the system bandwidth is limited by the RHP zero in the boost converter. The MHCC technique utilizes the characteristics of the RHP zero to cause a large control signal due to worse phase margin to rapidly recover the voltage level at the output of error amplifier. However, the worse phase margin can't ensure the stable operation in the steady state. The MHCC technique can adaptively adjust the compensation poles and zeros to low frequencies to guarantee the system stability. During the transient response, if i_c can rise and fall as soon as possible, the recovery time will be shortened as shown in Fig. 10(c).

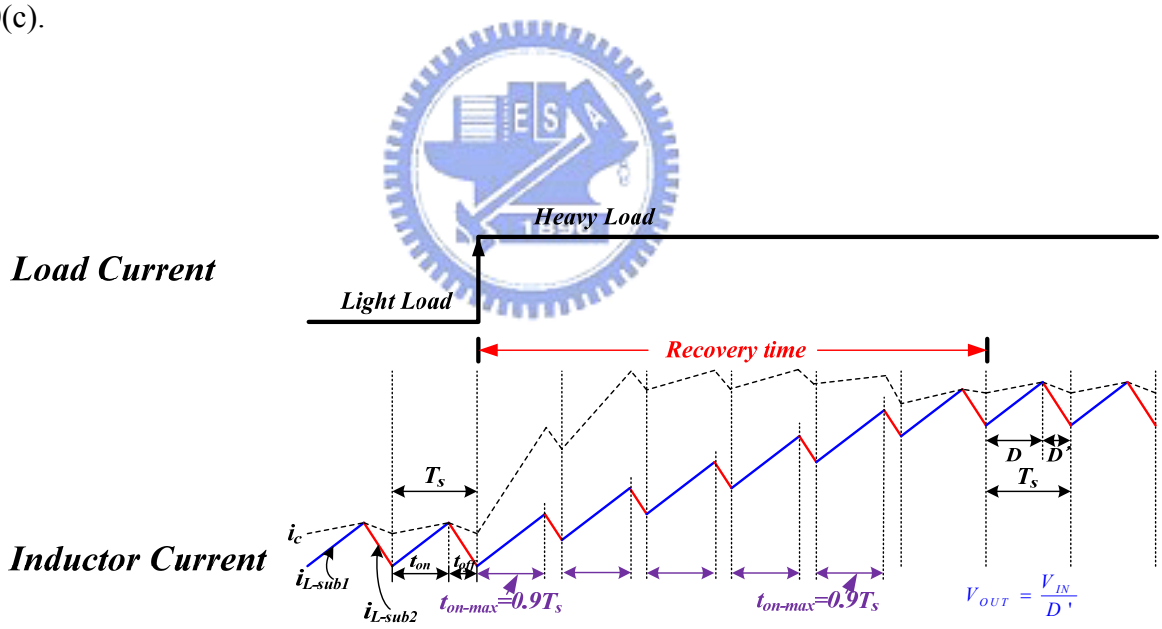

(a)

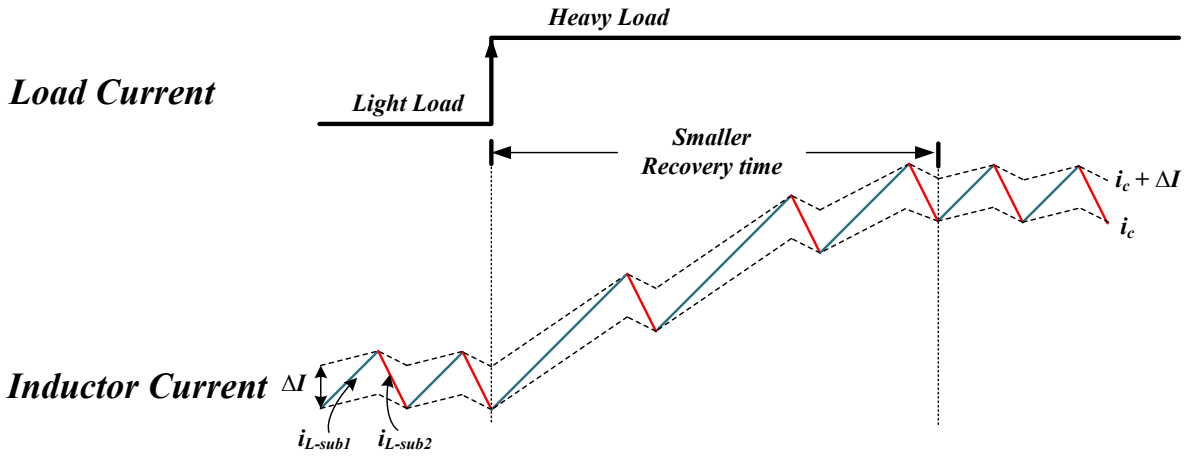

(b)

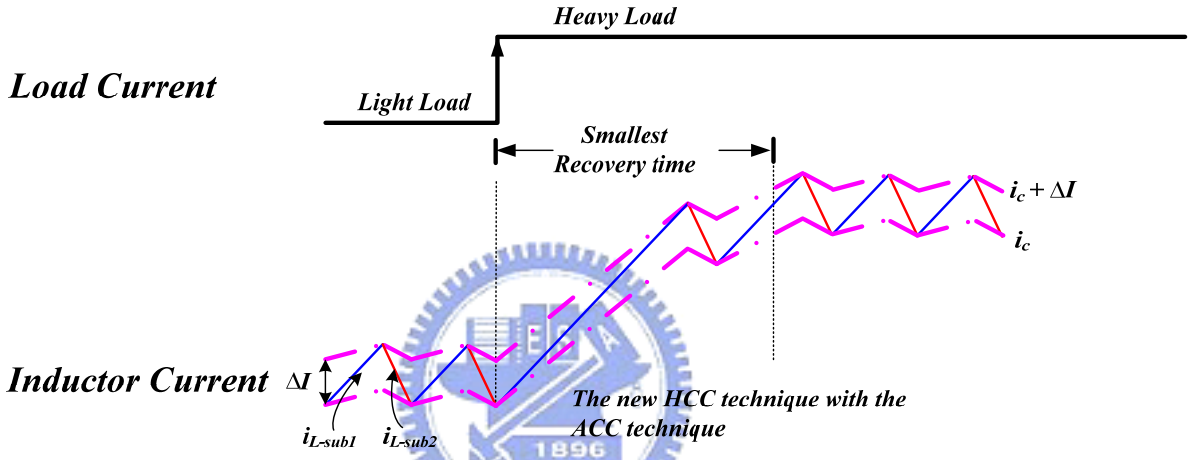

(c)

Fig. 10. Recovery time during light load to heavy load: (a) The waveforms controlled by the PWM technique. (b) The waveforms controlled only by the new HCC technique. (c) The waveforms controlled by the proposed MHCC technique.

Chapter 4

The Circuit Implementation

The proposed MHCC technique contains two main blocks. One is the HCC circuit and the other one is ACC circuit. The current sensor and the fixed hysteretic current window circuit constitute the HCC circuit. The adaptive compensation resistance and capacitance circuits and the ACC controller constitute the ACC circuit.

4.1 Current Sensor

The HCC technique needs to sense the full-range inductor current. Thus, an accurate current sensor is required. As depicted in Fig. 11, a small value of sensing resistor R_S is connected in series with the inductor to sense the full-range inductor current. It may cause a little reduction in the power conversion efficiency but it is a simple implementation. The transistors M_1 and M_2 are biased by the same current I_1. Thus, $V_{SG1}=V_{SG2}$. According to the current values labeled in the figure, (20) can be derived and simplified as (21) if $R_1=R_2$ under a good layout matching result.

$$V_{SG1}+(I_o+I_1)R_1=V_{SG2}+(I_L+I_1)R_S+I_1R_2 \tag{20}$$

$$I_o=I_L\frac{R_S}{R_1} \tag{21}$$

As a result, the sensing signal V_{SENSE} can be expressed in (22) and used to represent the full-range inductor current. Easily, the value of V_{SENSE} can be scaled by the ratio of (R_S*R_V) to R_1. According to the operation of the HCC technique, the value of V_{SENSE} is limited within the hysteresis window, which is controlled by the fixed hysteretic window circuit.

$$V_{SENSE} = I_o R_V = I_L \frac{R_S R_V}{R_1} \propto I_L \tag{22}$$

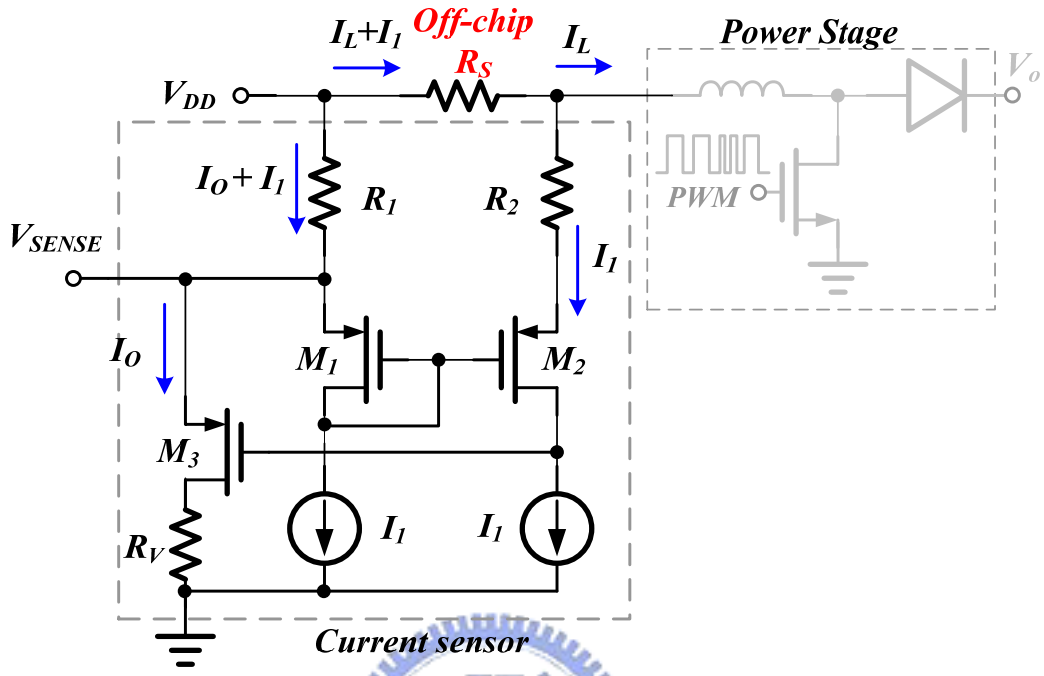

Fig. 11. The schematic of current sensor.

4.2 Fixed Hysteretic Current Window Circuit

In Fig. 12, the fixed hysteretic current window circuit is designed to accurately control the output ripple for ensuring the regulation performance. The low band of the fixed hysteretic current window is controlled by the output of the error amplifier, which is V_{eao}. Thus, a unity-gain buffer used to filter out the switching noise can generate the low band V_{IL}. The hysteretic window is easily generated by adding an IR-drop to the low band V_{IL}. The value of IR-drop is derived by a constant current flowing through a hysteresis resistor R_{hys}. As a result, the upper band V_{IH} can be expressed by (23). The cascaded current mirror M_6 and M_7 can suppress the channel length modulation effect to get a higher accuracy.

$$V_{IH} = V_{IL} + I_{N1} \times R_{hys} \tag{23}$$

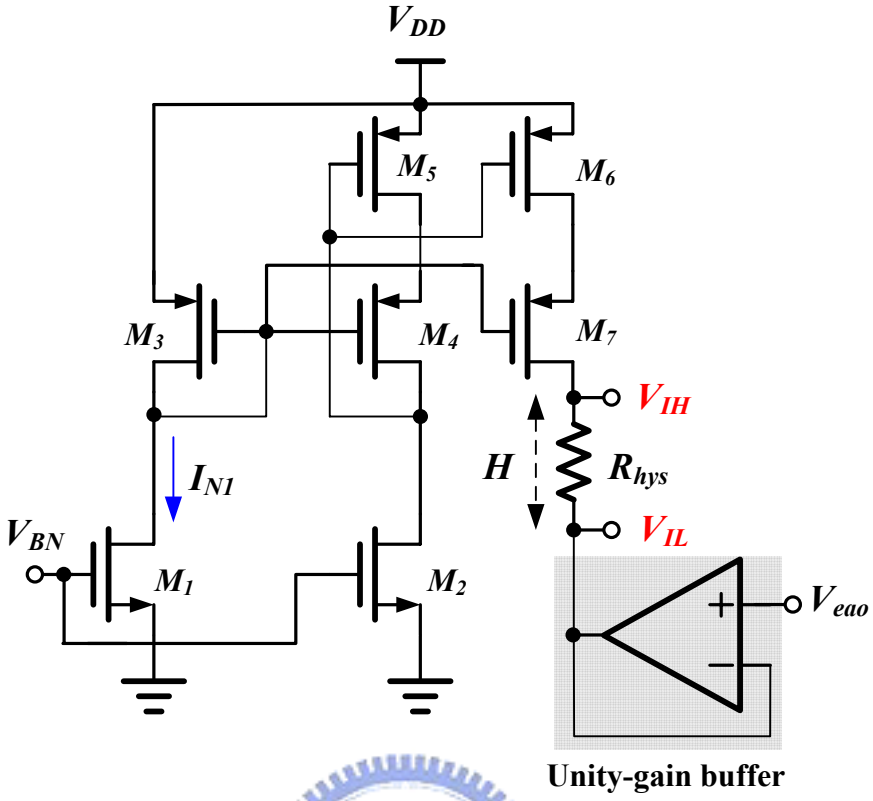

Fig. 12. The fixed hysteretic current window circuit.

4.3 The Adaptive Capacitance and Resistance Circuits and the ACC Controller

The fast transient mechanism is triggered by the threshold detector in Fig. 13(a). Once the feedback voltage V_{FB} is higher or lower than V_H or V_L, respectively, the ACC controller starts to control the fast transient procedure. The ACC technique can speed up the transient response by two transient procedures. One is transient 1 stage and the other is transient 2 stage. The transient 1 stage is simply decided by a one-shot circuit to rapidly increase the voltage of V_{eao}. As depicted in Fig. 13(a), the one-shot period can be determined by (24).

$$T_{one\text{-}shot} = \frac{C_S \cdot V_{ref}}{I_S + \frac{V_{DD}}{R_S} - g_m \cdot \left| V_{LP1} - V_{LP2} \right|} \tag{24}$$

The one-shot period is inversely proportional to the input voltage since the one-shot

value should be shortened under a large input voltage. Besides, a bigger overshoot output voltage and undershoot output voltage need a longer one-shot value. The time constant $R_S C_S$ can be adjusted by the trimming process to ensure the system stability at any loads.

The adaptive resistance is shown in Fig. 13(b) and equal to the value of two resistances in parallel. That is, $R_{Z1} = R_{LIGHT} \| R_{MN\_HEAVY}$. The maximum equivalent value of R_{Z1} is designed to R_{LIGHT} at light loads since the transistor M_{N_HEAVY} operating in cut-off region causes R_{MN_HEAVY} large to be ignored. The adaptive capacitance in Fig. 13(b) contains the voltage follower designed by the low-voltage operational amplifier to ensure the accurate current mirror constituted by the transistors $M_1 \sim M_4$. The input common mode range can be set from 0.4V to 1.9V. The current mirror array can determine the value of the pseudo capacitance C_{pseudo}. The ratio of the current mirror array is 1:M:N:(100-M-N). In this paper, M=65 and N=30. During the transient 1 stage, the switches in Fig. 13(b) are set by the table in Fig. 13(c).

Thus, C_{pseudo} changes from $(1+K)C_{Z1}$ to the value as shown in (25).

$$C_{pseudo} = \left(1 + \frac{100 - M - N}{1 + M + N}\right) C_{Z1} = \left(1 + \frac{100 - 65 - 30}{1 + 65 + 30}\right) \times 2pF \approx 2.1pF \tag{25}$$

That is, 95% of the mirrored current is directed to the small capacitor C_{Z1} to rapidly increase the voltage level of V_{eao}. As a result, the system bandwidth can be extended and the drop voltage can be reduced. However, the phase margin is not enough to ensure a stable operation. Thus, the one-shot timing control in (24) depends on V_{in} and V_o to avoid oscillating.

After the transient 1 stage, the transient 2 stage is determined by the valley of the output voltage. Thus, a peak detector in Fig. 13(a) is required to decide the period of the transient 2 stage. As illustrated in Fig. 13(d), the feedback signal V_{FB} can be filtered by two low-pass filters, which are (R_{LP1}, C_{LP1}) and (R_{LP2}, C_{LP2}), to generate two output signals V_{LP1} and V_{LP2}. In the transient 2 stage, the switches in Fig. 13(b) are conservatively set to increase C_{pseudo} to the value as shown in (26).

$$C_{pseudo} = \left(1 + \frac{100 - N}{1 + N}\right) C_{Z1} = \left(1 + \frac{100 - 30}{1 + 30}\right) \times 2pF \approx 6.5pF \tag{26}$$

During the transient 2 stage, the compensation poles and zeros are pulled toward the origin to get a higher PM value. Once V_{LP1} is higher than V_{LP2}, the transient 2 stage is ended. After the detection of the peak value, the compensation poles and zeros are set to the positions that can guarantee an adequate PM value. C_{pseudo} is equal to $(1+K)C_{Z1}$, again.

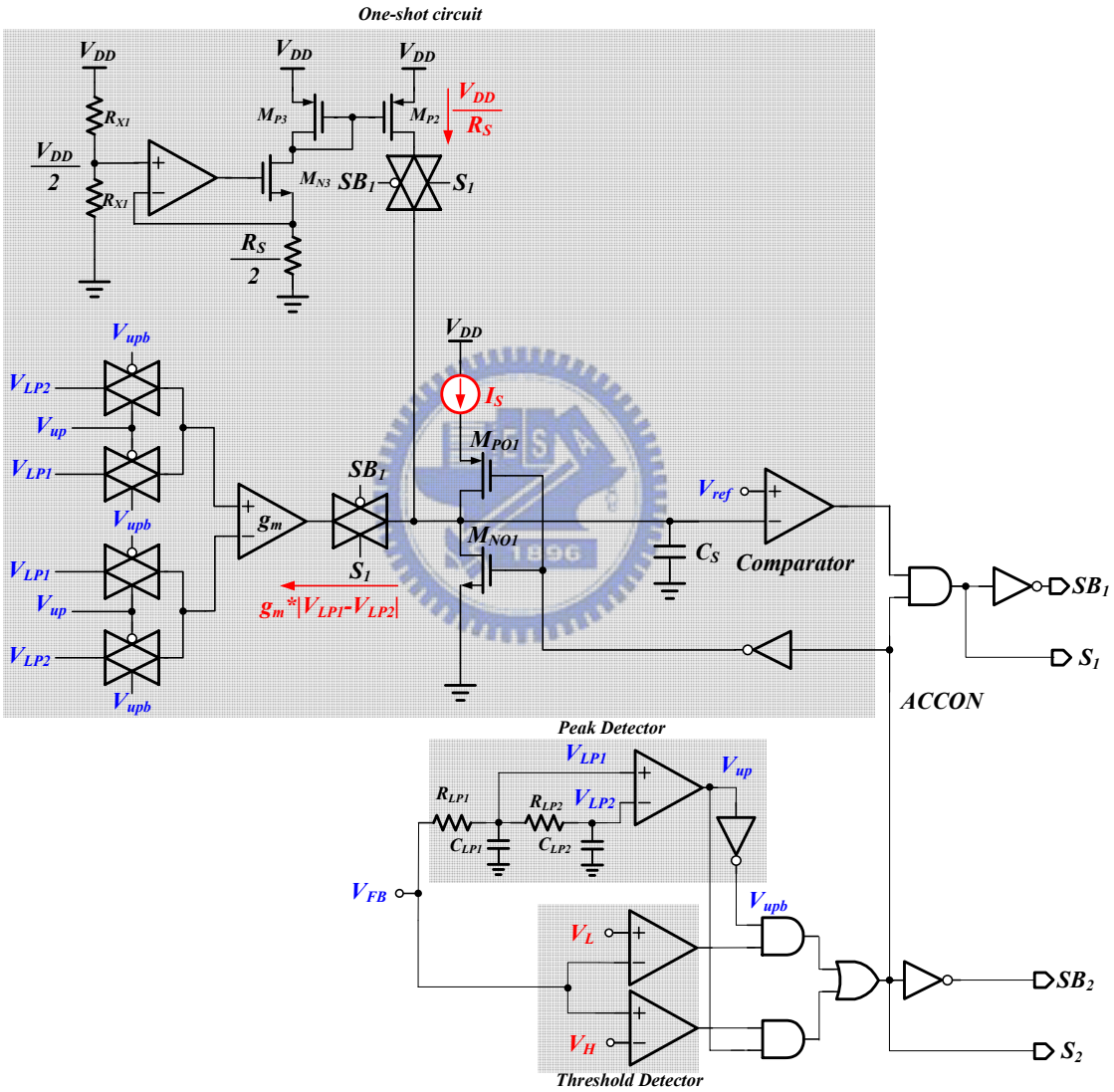

(a)

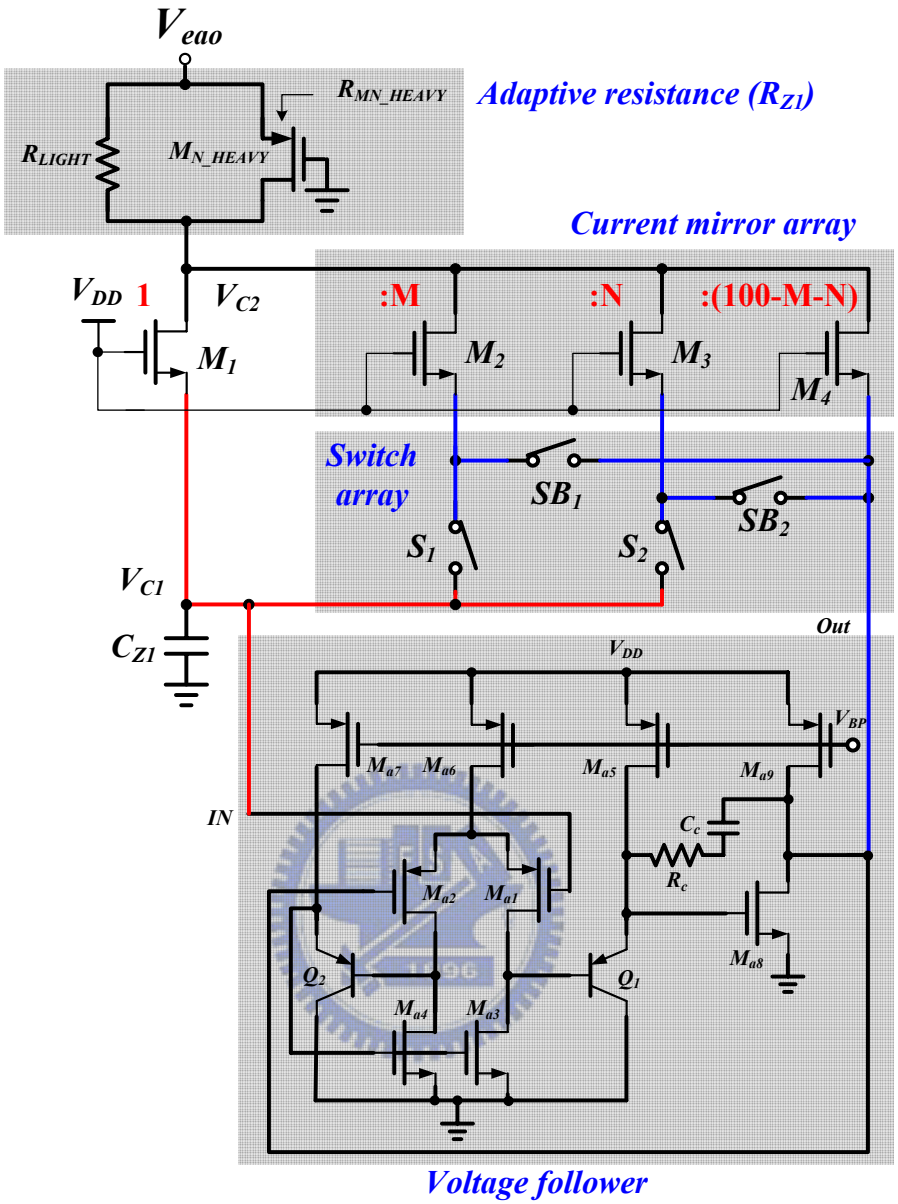

(b)

	S_1 (SB_1)	S_2 (SB_2)
Initial state	OFF (ON)	OFF (ON)
Transient 1	ON (OFF)	ON (OFF)
Transient 2	OFF (ON)	ON (OFF)
Final state	OFF (ON)	OFF (ON)

(c)

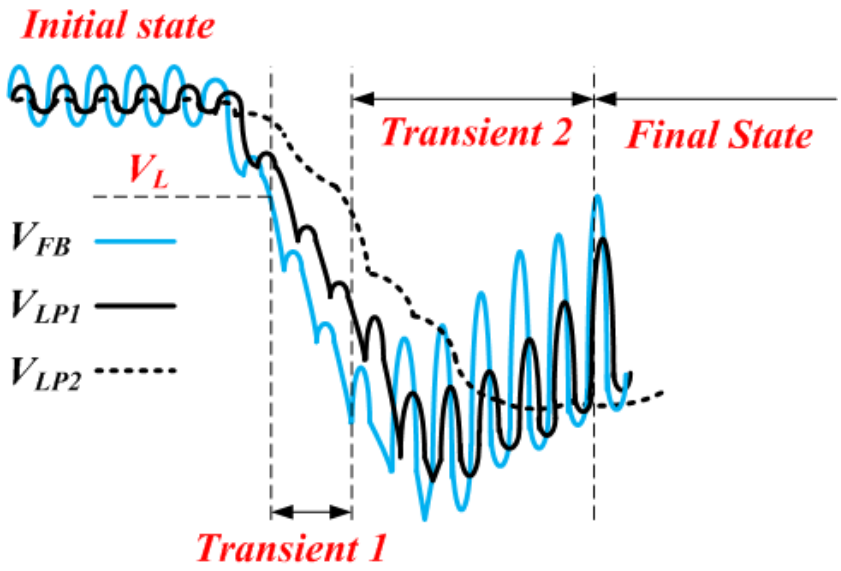

(d)

Fig. 13. (a) The schematic of the ACC controller. (b) The adaptive capacitance circuit. (c) The controlling table of the switches. (d) The waveforms of the peak detector.

In Fig. 14(a), the Bode plot is shown when load current changes from light to heavy. Besides, the position of all poles and zeros is listed in Fig. 14(b). The value of f_c is set to about 30% of the value of $f_{z(RHP)}$ at heavy loads. It has been mentioned in Fig. 4(b). Similarly, the Bode plot is shown in Fig. 15(a) when load current changes from heavy to light. Fig. 15(b) lists the relationship of the poles and zeros. At light loads, the value of f_c is set to about 30% of the value of f_{pc2}. The adaptive resistance moves both f_{zc1} and f_{pc2} toward the origin. Thus, f_{pc2} is smaller than $f_{z(RHP)}$ at light loads. In other words, f_{pc2} determines the position of f_c.

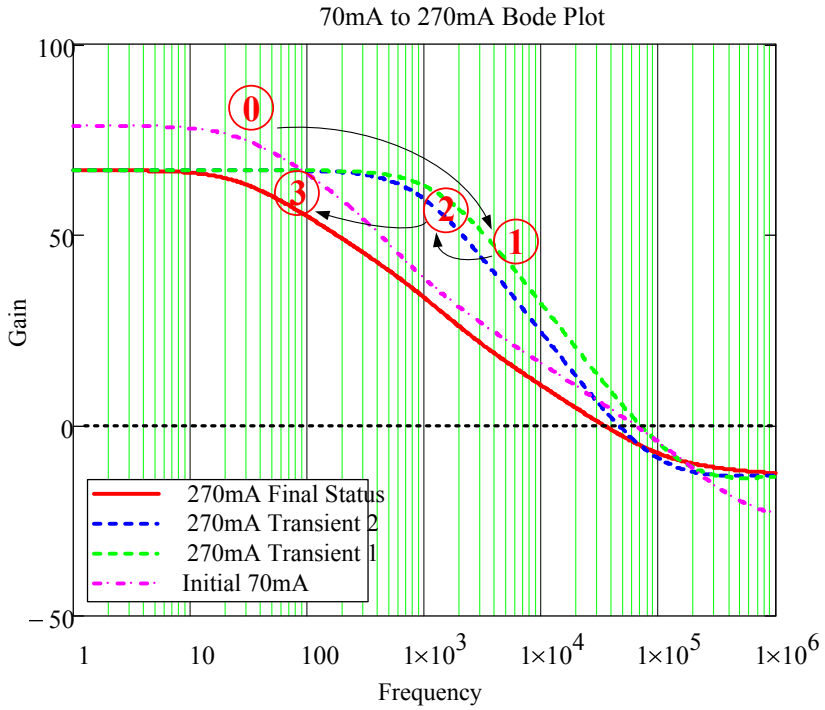

(a)

Status	Dominant-pole (f_{pc1})	Output stage-pole (f_{p1})	Zero (f_{zc1})	High freq. pole (f_{pc2})	**RHP zero** ($f_{z(RHP)}$)	ESR zero ($f_{z(ESR)}$)	DC Gain (dB)	UGF	Phase (deg)
⓪ Light Load (70mA)	25	273	916	191K	**446K**	468K	78.6	63K	71
Output load current changes from light (70mA) to heavy load (270mA).									
① Transient 1	1.7K	1.1K	225K	700K	**116K**	468K	66.9	70K	-9
② Transient 2	701	1.1K	73K	550K	**116K**	468K	66.9	45K	13
③ Heavy Load (270mA)	26	1.1K	1.8K	377K	**116K**	468K	66.9	34K	71

(b)

Fig. 14. (a) The Bode plot when load current changes from light to heavy. (b) The position of all poles and zeros.

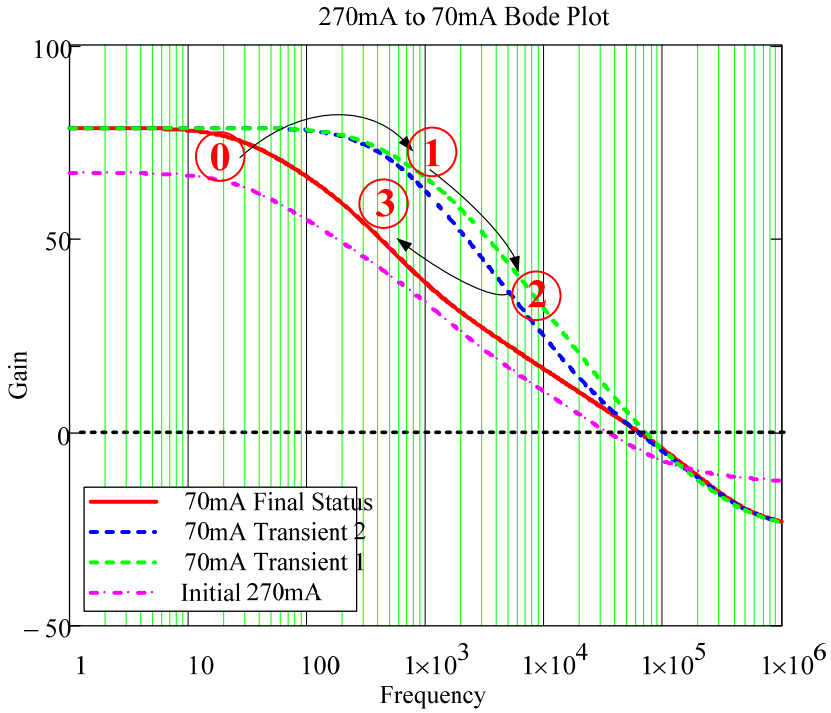

(a)

Status	Dominant-pole (f_{pc1})	Output stage-pole (f_{p1})	Zero (f_{zc1})	High freq. pole (f_{pc2})	**RHP zero** ($f_{z(RHP)}$)	ESR zero ($f_{z(ESR)}$)	DC Gain (dB)	UGF	Phase (deg)
⓪ Heavy Load (270mA)	26	1.1K	1.8K	377K	116K	468K	66.9	34K	71
Output load current changes from heavy (270mA) to light (70mA) load.									
① Transient 1	1.7K	273	88K	277K	446K	468K	78.6	70K	25
② Transient 2	692	273	28K	218K	446K	468K	78.6	61K	50
③ Light Load (70mA)	25	273	916	191K	446K	468K	78.6	63K	71

(b)

Fig. 15. (a) The Bode plot when load current changes from heavy to light. (b) The position of all poles and zeros.

4.4 The Start-up Circuit and the Protection Circuits

The flow chart as depicted in Fig. 16(a) includes the start-up operation, the protection functions, and the MHCC operation. When the power is turned on, the chip begins the start-up procedure. As a result, it is necessary to have the under-voltage lockout (UVLO) circuit as shown in Fig. 16(b) to determine whether the power supply is greater than 2.5V or not. If the supplying voltage is not high enough, the closed-loop is not adequate to be established in order to avoid oscillating. Before the supplying voltage approaches the pre-defined voltage level, the value of *UVLO* is high and can be expressed as (27).

$$UVLO = 1 \text{ when } V_{in} < V_{ref} \cdot \frac{R_{U1} + R_{U2}}{R_{U2}} \tag{27}$$

In this paper, the supplying voltage should be larger than 2.5V to guarantee a stable closed-loop operation. Before the closed-loop operation, the output is connected to the input supplying voltage through the inductor. Once the power supply is greater than 2.5V, the start-up circuit takes over the operation. That is the switching converter will begin to boost the output to a higher output voltage level. During this start-up procedure, the maximum inductor current $I_{L\_max\_startup}$ is limited below 1.13A.

In the implementation of the start-up circuit, it is easy to divide the resistor R_V in Fig. 11 into three small resistors, R_{V1}~R_{V3} in Fig. 16(b). Good layout matching can guarantee the accuracy the current sensing and the protection function. According to (21), the divided voltage V_{ST} at node X can be used to limit the inductor current during the start-up period. Thus, the value of $I_{L\_max\_startup}$ can be expressed as (28).

$$I_{L\_max\_startup} = V_{ref} \cdot \frac{R_1}{R_S \cdot (R_{V1} + R_{V2})} \tag{28}$$

When the output voltage V_o approaches to 12V, the feedback voltage V_{FB} will be greater than V_{ref}. The signal *ST_OK* at the output of the D flip-flop will be set to high to enter the

MHCC operation. The maximum inductor current will be raised to a higher level to avoid the overloading condition during the MHCC operation. The voltage V_{OCP} at node Y is used to compare with V_{ref} to detect the over current protection (OCP) condition and thus the protection current of the OCP protection is higher than that of the start-up period. The expression of OCP is shown in (29). When the OCP condition occurs, the *ST_OK* will be set to 0 and the high voltage (HV) N-MOSFET, *HN24G5*, will be turned off to let the system return to the start-up operation.

$$OCP = 1 \text{ when } I_o \times R_{V2} > V_{ref} \tag{29}$$

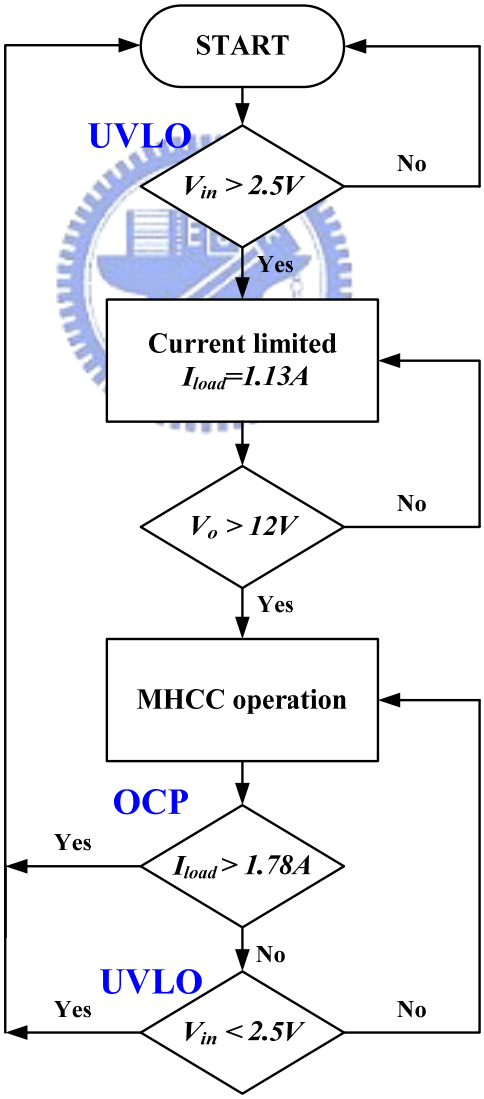

(a)

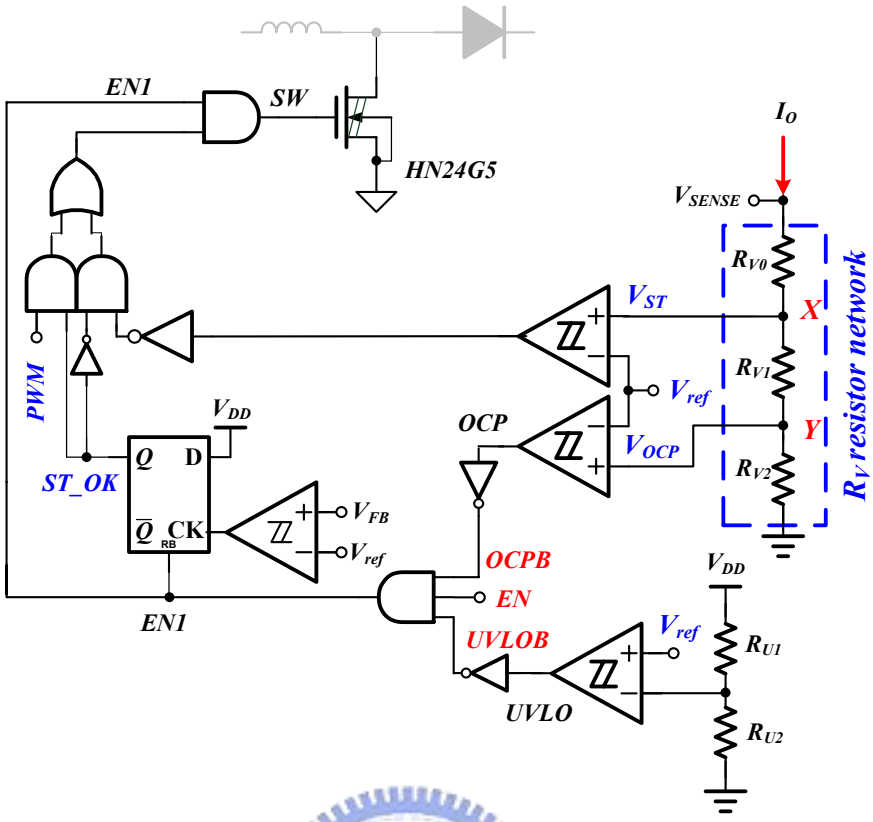

Fig. 16. (a) The flow chart includes the start-up operation, the protection functions, and the MHCC operation. (b) The start-up and protection circuits.

Chapter 5

Experimental Results

The proposed boost convert with the MHCC technique was fabricated by TSMC 0.25 μm CMOS process. The threshold voltages of nMOSFET and pMOSFET are 0.477 V and -0.596 V, respectively. The off-chip inductor and output capacitor are 6.8 μH and 10 μF, respectively. The output voltage V_o is 12V to drive 3 white LEDs in series. The specification is listed in Table I. The chip micrograph is shown in Fig. 17 and the chip area is about 1480 μm × 2780 μm including the test pads.

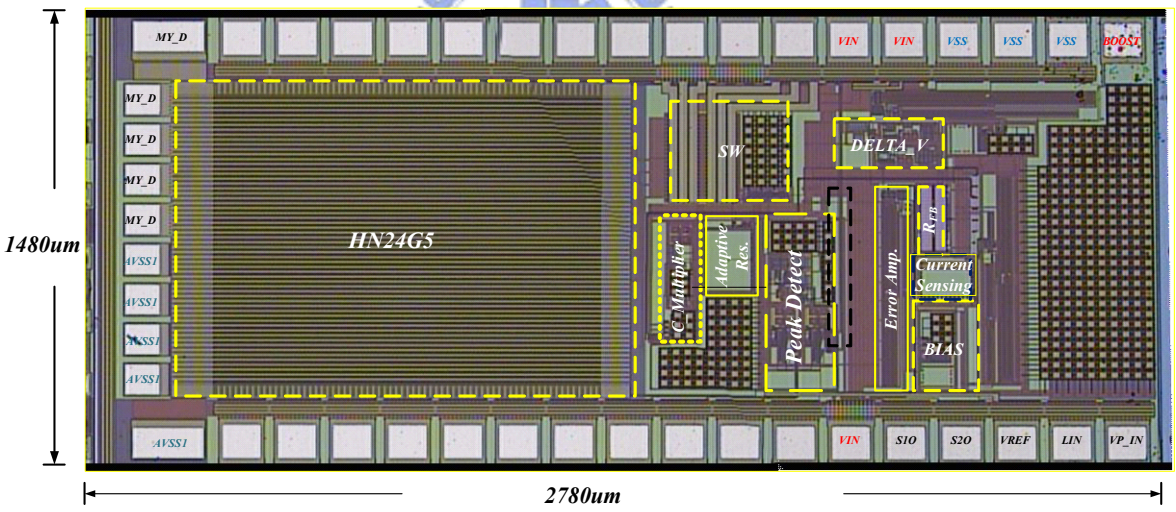

Fig. 17. Chip micrograph.

TABLE I THE DESIGN SPECIFICATION

Characteristics	*Typ.*	*Unit*
Supply Voltage (V_{in})	*3.5~4.5*	*V*
Output Voltage (V_o)	*12*	*V*
Output Current (I_{load})	*70~270*	*mA*

Input Inductor (L)	*6.8*	*μH*
Equilibrium series Resistance of the inductor (DCR)	*45*	*mΩ*
Output capacitor (C_O)	*10*	*μF*
Equilibrium series resistance of the output capacitor (R_{ESR})	*50*	*mΩ*
Operation temperature	*0~100*	*℃*

Experimental results of conventional boost converter are shown in Fig. 18. The input voltage is 4V. The load current changes from 70mA to 270mA. The slew rate of load current is 200mA/us. The undershoot voltage and overshoot voltage are 338mV and 308mV, respectively. The recovery time is 141μs when load current changes from light to heavy load or heavy to light. And the load regulation is 0.16mV/mA. It is obvious to see that the bandwidth is limited by the existence of the RHP zero. Under the low-bandwidth design, the transient response can't be speeded up. Thus, the slow-response output voltage may cause the LEDs in series have a little of luminance variation when the dimming control is applied on the LED brightness control.

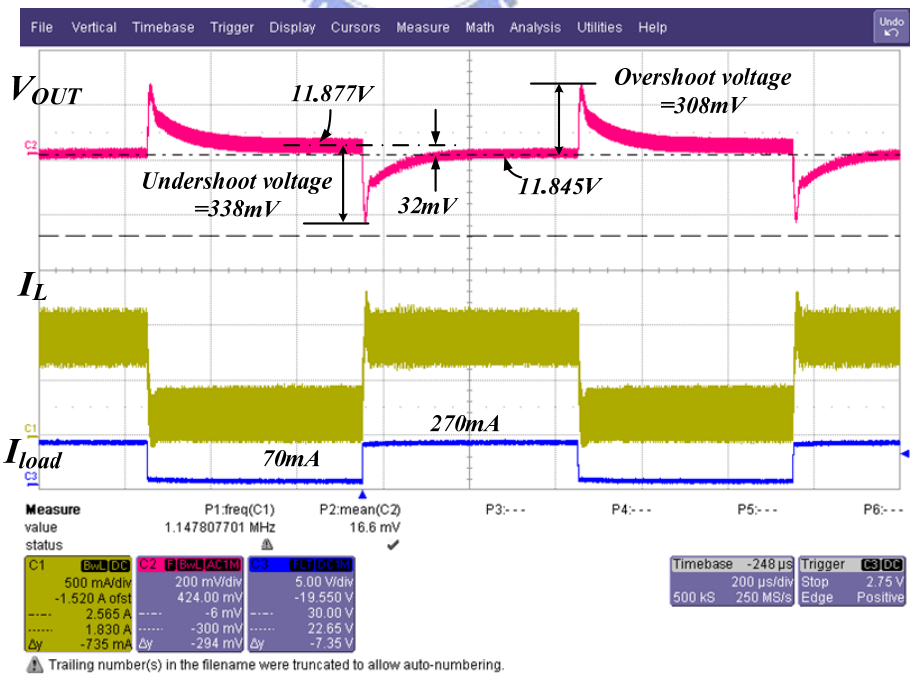

(a)

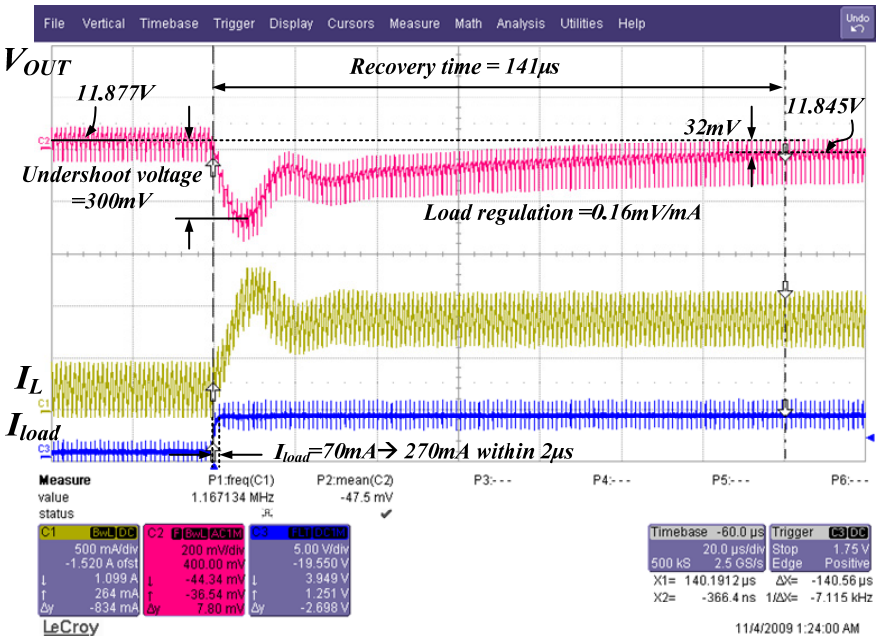

(b)

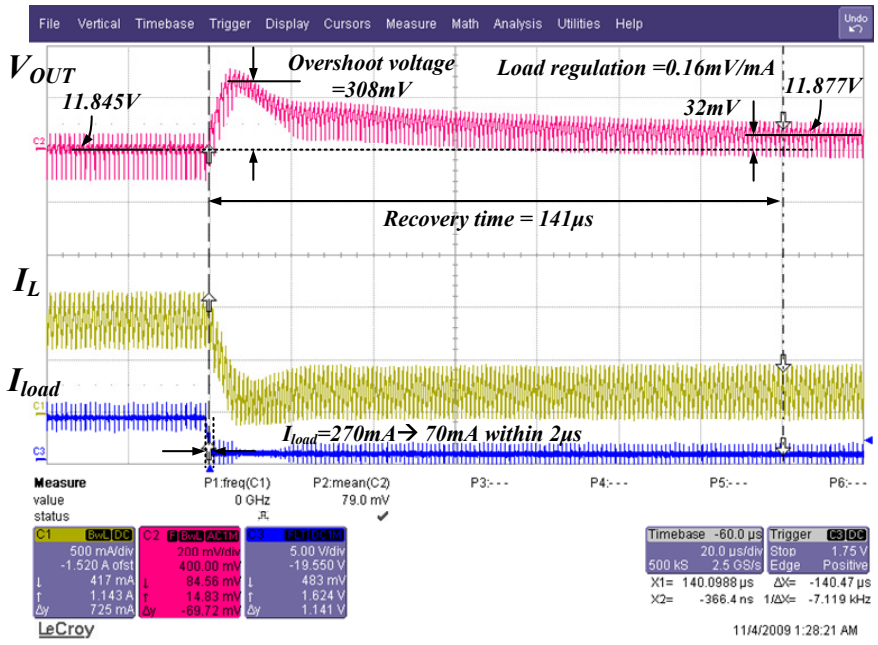

(c)

Fig. 18. Waveforms in conventional boost converter with hysteresis control when load current changes from 70mA to 270mA within 2µs.

Compared to the slow-response of the conventional design, the experimental results of the proposed boost converter are shown in Fig. 19. The test setting is the same as the conventional design. The undershoot voltage and overshoot voltage are 300mV and 234mV, respectively. The recovery time of light load to heavy load is 19.5µs and the recovery time of

heavy load to light load is 18.8μs. Experimental results show the improvement in transient response is higher than 7.2 times when load current changes from light to heavy or vice versa compared to the conventional boost converter design. The improvement comes from the new HCC and the ACC techniques. The output of the error amplifier can be settled rapidly by the ACC technique to define the low band of the hysteresis window. Besides, the new HCC technique can adaptively adjust the on-time and off-time values to speed up the transient response time. The load regulation, which is 0.11mV/mA, is also better than that of the conventional design due to the ACC technique.

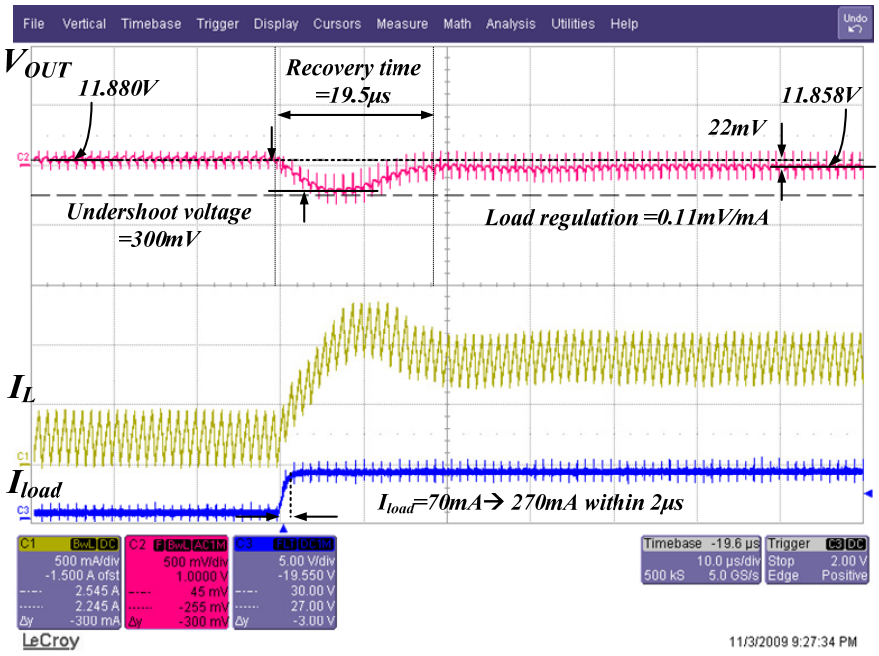

(a)

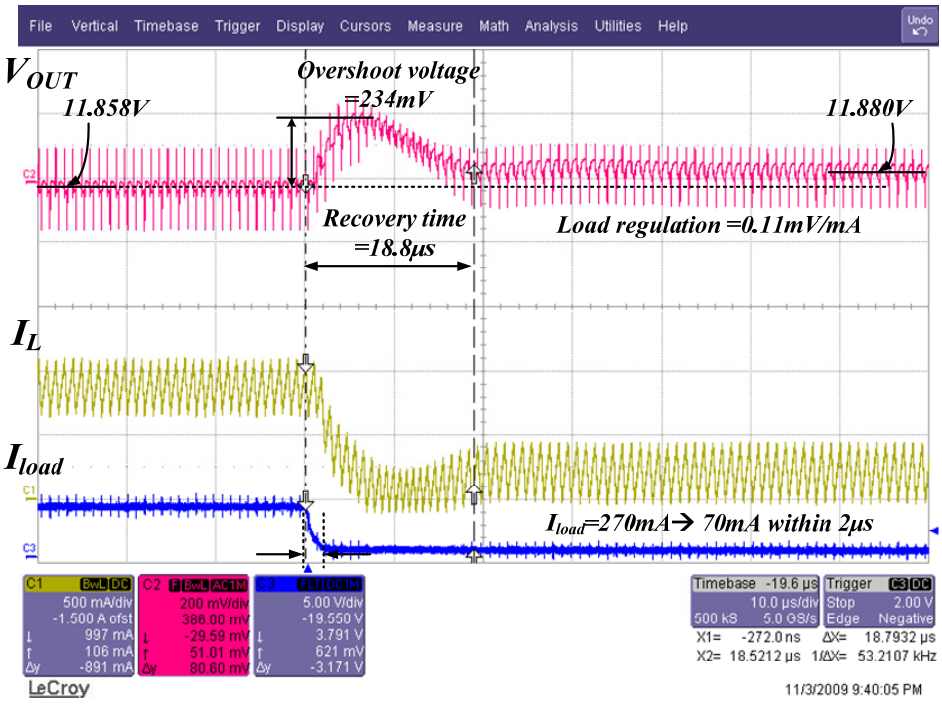

(b)

Fig. 19. Waveforms in the proposed boost converter with the MHCC technique (a) when load current changes from 70mA to 270mA within 2μs and (b) when load current changes from 270mA to 70mA within 2μs.

The experimental results of the proposed boost converter are shown in Fig. 20 when the load current changes from 70mA to 220mA or vice versa. The fast transient performance can be easily seen since the MHCC technique can speed up the transient response over a wide load current range. Certainly, the fast transient performance has its limitation. The load current step decreases to about 100mA and 50mA as shown in Fig. 21 (a) and (b), respectively. The transient response time has a little improvement compared to that of the large load current step since the ACC technique has only a little effect on the whole system. Fortunately, the ACC technique consumes a little power since it works only when the output voltage has a large variation. Fig. 22 shows the power conversion efficiency. It demonstrates that the power conversion efficiency is nearly not influenced with or without the ACC technique. The power consumption overhead is merely 1%. The maximum power conversion efficiency is about 90%. The start-up waveforms are also shown in Fig. 23. The comparison

summary between the conventional and the proposed MHCC techniques is listed in TABLE II.

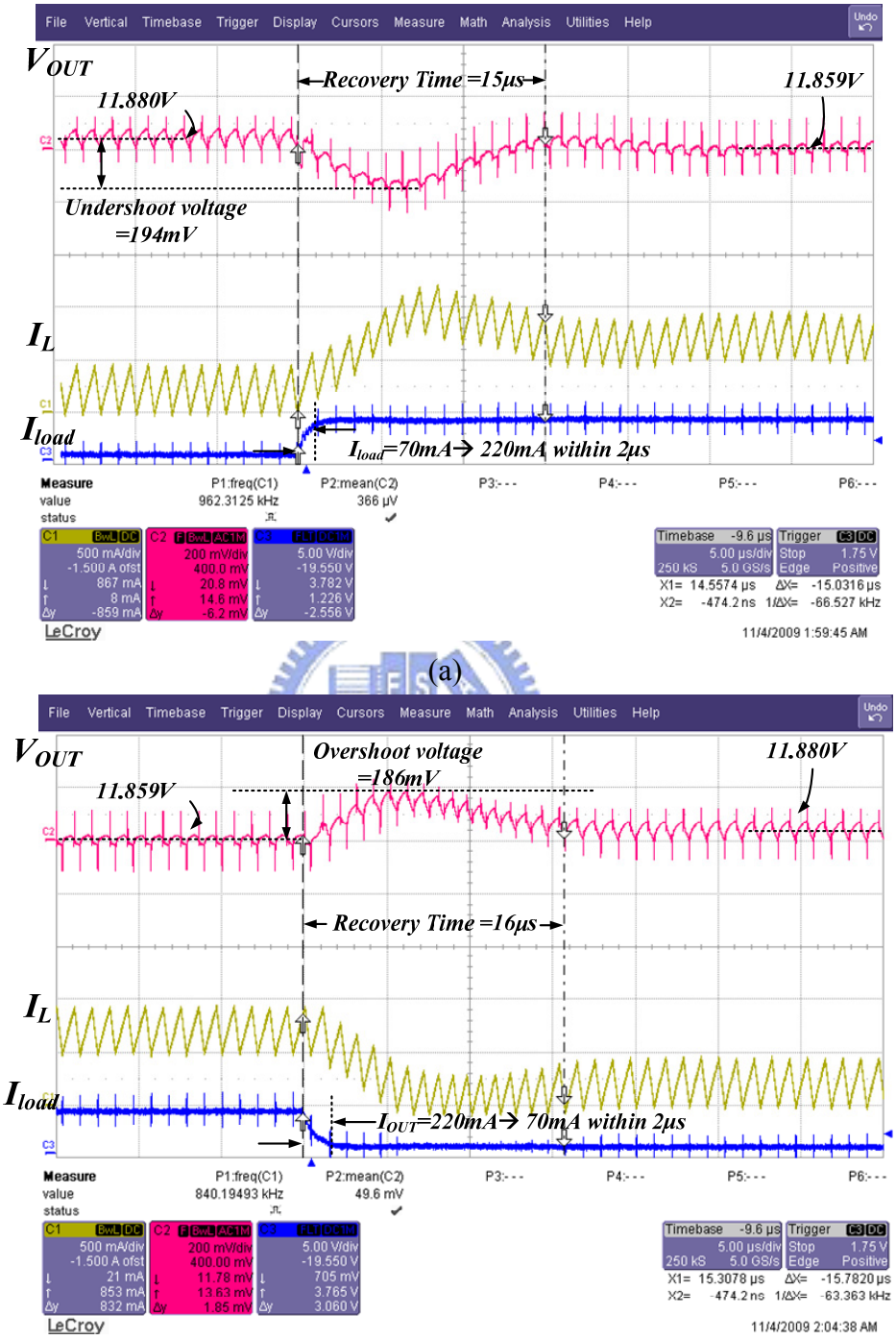

Fig. 20. Waveforms in the proposed boost converter with the MHCC technique when load current changes from 70mA to 220mA within 2μs.

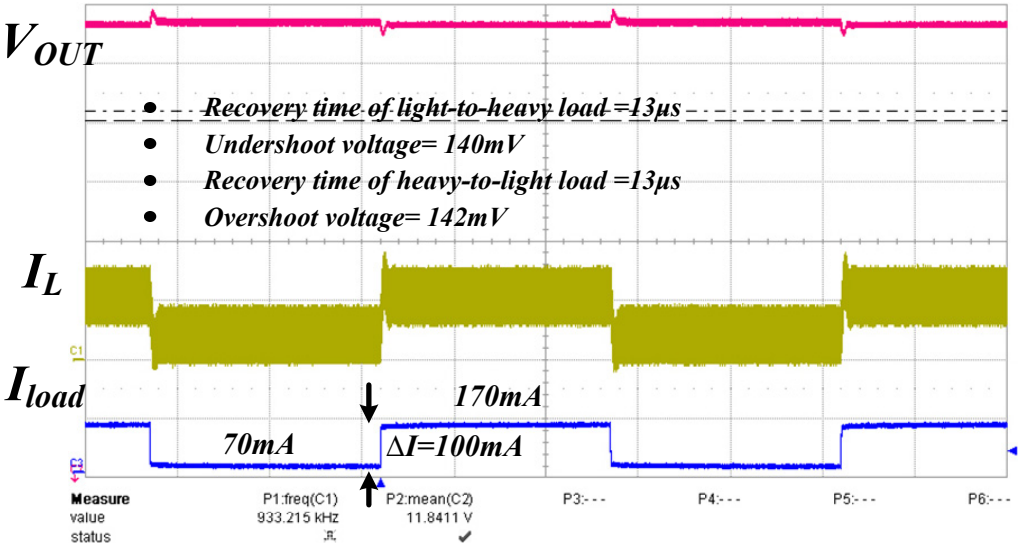

(a)

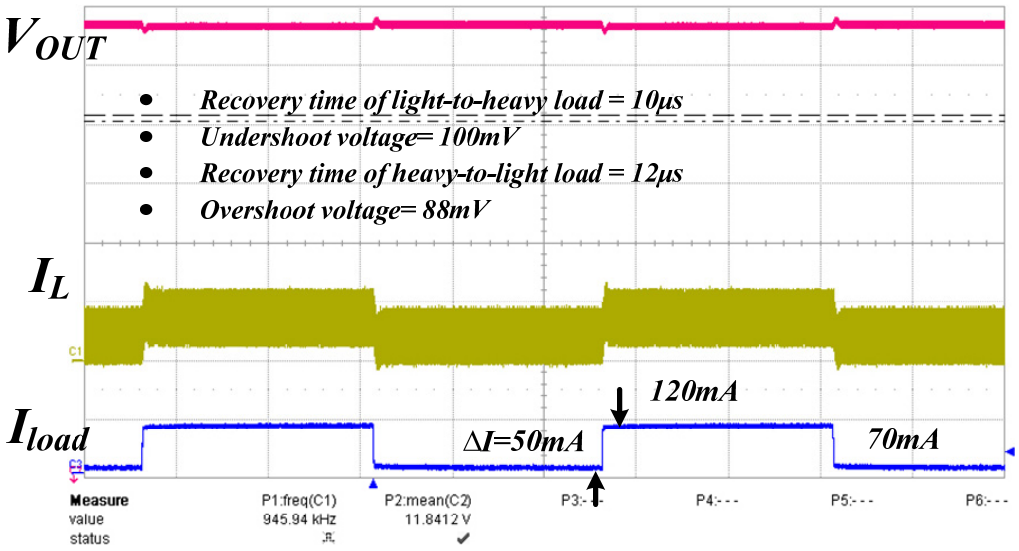

(b)

Fig. 21. Waveforms in the proposed boost converter with the MHCC technique when load current changes from light to heavy within 2μs.

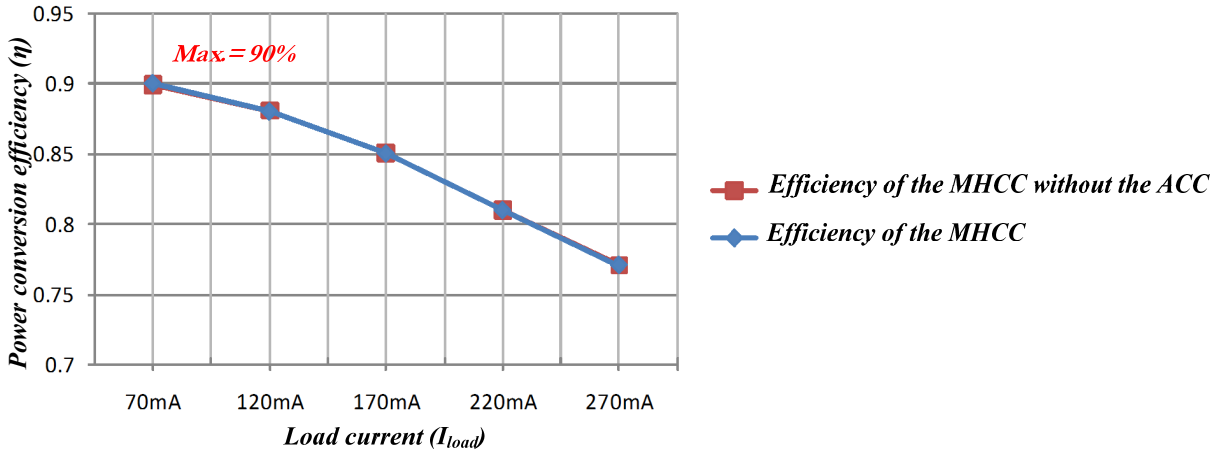

Fig. 22. Power conversion efficiency.

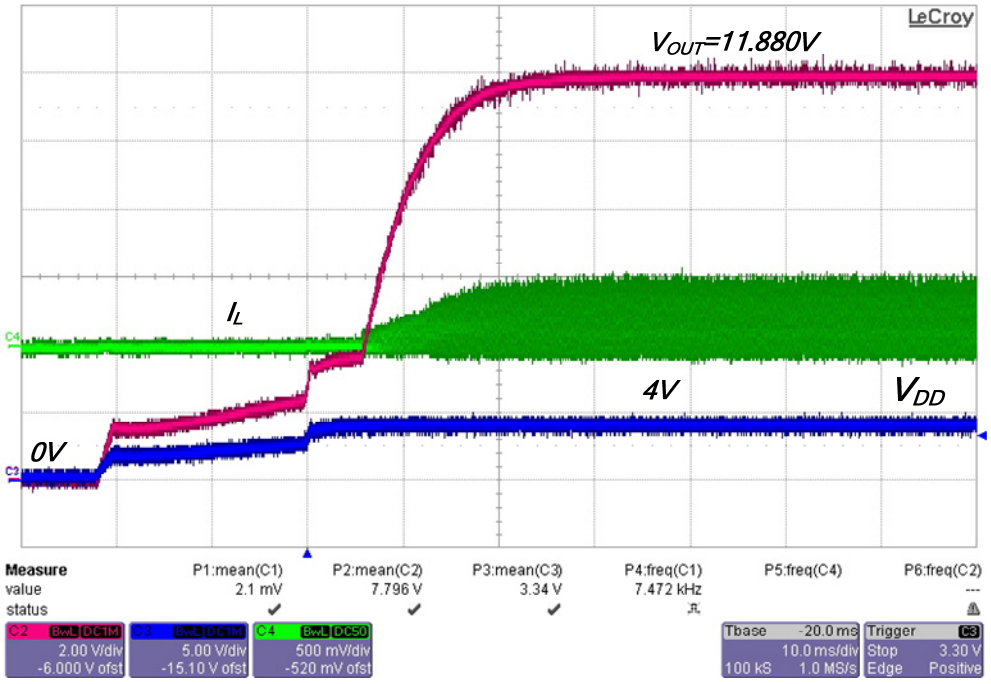

Fig. 23. The start-up waveforms when the input voltage is slowly ramped up and the output loading is 70mA.

TABLE II THE SUMMARIES OF THE CONVENTIONAL AND MHCC TECHNIQUES

Characteristics	***Conditions***	***MHCC Technique***	***Conventional Technique***
Supply Voltage	--	*4V*	*4V*
Output Voltage	--	*12V*	*12V*
Output Current Variation	--	*200mA*	*200mA*
Overshoot Voltage	I_{load}=*270mA→70mA within 2μs*	*234mV*	*308mV*
Undershoot Voltage	I_{load}=*70mA→270mA within 2μs*	*300mV*	*338mV*
Recovery time of heavy-to-light load	I_{load}=*270mA→70mA @ 0.1% rated voltage within 2μs*	*18.8μs*	*141μs*
Recovery time of light-to-heavy load	I_{load}=*70mA→270mA @ 0.1% rated voltage within 2μs*	*19.5μs*	*141μs*
Load Regulation	--	*0.11mV/mA*	*0.16mV/mA*

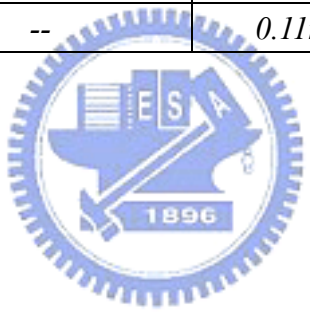

Chapter 6

Conclusion

This paper proposes a modulated hysteretic current control (MHCC) technique to improve transient response of DC-DC boost converters, which suffer from low bandwidth due to the existence of right-half-plane (RHP) zero. The new HCC technique can adaptively adjust the on-time and off-time values of the PWM waveform to speed up the transient response. Besides, the ACC technique can settle the low band value of the hysteresis generated by the error amplifier to further improve the transient response. Thus, the low-bandwidth and large overshoot and undershoot voltages due to the RHP zero can be improved. The proposed boost converter with the MHCC technique fabricated by TSMC CMOS 0.25 um process can demonstrate the fast transient performance to verify its advantage in the driving capability of the LEDs in series. A good driving capability and accuracy can be guaranteed by the proposed MHCC technique according the fast transient performance in the experimental results.

6.1 Future Work

The MHCC technique also minimizes the external components and thus it has the advantage of small footprint. But the MHCC has the same disadvantage of the complex design the EMI filters. Therefore, the improvement of EMI issue is important in the future.

Reference

[1] Huang-Jen Chiu and Shih-Jen Cheng, "LED Backlight Driving System for Large-Scale LCD Panels," *IEEE Trans. Ind. Electron.,* vol. 54, pp. 2751-2760, Oct. 2007.

[2] ln-Hwan Oh, "A single-stage power converter for a large screen LCD back-lighting," in *Proc. IEEE APEC*, pp. 1058-1063, March 2006.

[3] G. Jurasek, G. Levin, P. Sisson, and S. Repplinger, "High Efficiency Automotive Power Supply with Hysteretic Current Mode Controller," in *Proceedings of IEEE Applied Power Electronics Conference and Exposition*, vol. 2, pp. 861, March 1996.

[4] Robert W. Erickson and Dragan Maksimovic, *Fundamentals of Power Electronics*, 2nd ed., Norwell, MA: Kluwer Academic Publishers, 2001.

[5] Wei Tang, Fred C. Lee, "Small-Signal Modeling of Average Current-Mode Control," *IEEE Trans. Power Electron.*, vol. 8, pp. 112-119, Apr. 1993.

[6] Hong-Wei Huang, Ke-Horng Chen, and Sy-Yen Kuo, "Dithering Skip Modulation, Width and Dead Time Controllers in Highly Efficient DC-DC Converters for System-on-chip Applications," *in IEEE Journal of Solid-State Circuits,* pp. 2451-2465, Nov. 2007.

[7] J. H. Park and B. H. Cho, "Small Signal Modeling of Hysteretic Current Mode Control Using the PWM Switch Model," *IEEE COMPEL*, pp. 225-230, July 2006.

[8] B. Bryant and M. K. Kazimierczuk, "Small-signal duty cycle to inductor current transfer function for boost PWM DC-DC converter in continuous conduction mode," *IEEE ISCAS*, pp. 856-859, May 23-26, 2004.

[9] R. D. Middlebrook, "Modeling current-programmed buck and boost regulators," *IEEE Trans. Power Electron.*, vol. 4, pp. 36-52, Jan. 1989.

[10] R. B. Ridley, “A new, continuous-time model for current-mode control,” *IEEE Trans. Power Electron.*, vol. 6, pp. 271-280, April 1991.

[11] Chia-Jung Chang and Ke-Horng Chen, “Bidirectional Current-Mode Capacitor Multiplier in DC-DC Converter Compensation,” *IWSOC*, pp. 111-116, July 2005.

[12] G. A. Rincón-Mora, “Active Capacitor Multiplier in Miller-Compensated Circuits,” *IEEE J. Solid-State Circuits*, vol. 35, pp. 26–32, Jan. 2000.

[13] Ming-Hsin Huang and Ke-Horng Chen, “Single-Inductor Dual-Output DC-DC Converters with High Light-Load Efficiency and Minimized Cross-Regulation for Portable Devices,” *in IEEE Journal of Solid-State Circuits,* pp. 1099 - 1111, April 2009.

[14] Chao-Hsuan Liu, Yu-Chiao Hsieh, Ting-Jung Tai, and Ke-Horng Chen, “SAR-Controlled Adaptive (SARCA) Off-time Control without Sensing Resistor for Achieving 94% Efficiency and 98% Accuracy,” *in IEEE Transactions on Circuits and Systems I, June.* 2010.

[15] Feng Su, Wing-Hung Ki and Chi-Ying Tsui, “Ultra Fast Fixed-Frequency Hysteretic Buck Converter With Maximum Charging Current Control and Adaptive Delay Compensation for DVS Applications,” *IEEE J. Solid-State Circuits*, vol. 43, pp. 815-822, Apr. 2008

[16] Ding Ge, Zhiliang Chen, “On-chip boost DC-DC converter in color OLED driver & controller ICs for mobile application,” IEEE ASICON, vol. 1, pp. 459 – 463, Oct. 2005.

[17] Tin-Jong Tai and Ke-Horng Chen, “Switching Loss Calculation (SLC) and Positive/Negative Compensated Dynamic Droop Scaling (PNC-DDS) Technique for High-Efficiency Multiple-Input Single-Output (MISO) Systems,” in *IEEE Transaction on Power Electronics,* pp. 1386 - 1398, May 2009.

[18] V. Gupta, and G. A. Rincón-Mora, “Analysis and Design of Monolithic High PSR, Linear Regulators for Soc Applications,” *IEEE SOC Conference*, pp. 311-315, Sept.

2004.

[19] S. K. Hoon, S. Chen, F. Maloberti, J. Chen, and B. Aravind, “A low noise, high power supply rejection low dropout regulator for wireless system-on-chip applications,” *IEEE Custom Integrated Circuits Conference*, pp. 759-762, Sept. 2005.